Journal of South American Earth Sciences 88 (2018) 621–641

Contents lists available at ScienceDirect

Journal of South American Earth Sciences

journal homepage: www.elsevier.com/locate/jsames

Petrology and geochronology (U—Pb) OF the Caapucú suite – Southern Paraguay: POST-TECTONIC magmatism of the Paraguari belt

Amanda Figueiredo Granja Dorilêo Leite[a,c,*], Maria Zélia Aguiar de Sousa[b,c], Amarildo Salina Ruiz[b,c], Narciso Cubas[d], João Batista de Matos[b,c], Elton Luiz Dantas[e], Juliana Rezende de Oliveira[f,c]

[a] Programa de Pós-Graduação em Geociências, Universidade Federal de Mato Grosso (UFMT), Avenida Fernando Correa da Costa, s/n, CEP: 78.060-900, Cuiabá, MT, Brazil
[b] Faculdade de Geociências (FAGEO-UFMT), Avenida Fernando Correa da Costa, s/n, CEP: 78.060-900, Cuiabá, MT, Brazil
[c] Grupo de Pesquisa em Evolução Crustal e Tectônica-Guaporé (FAGEO-UFMT), Avenida Fernando Correa da Costa, s/n, CEP: 78.060-900, Cuiabá, MT, Brazil
[d] Facultad de Ciencias Exactas y Naturales, Departamento de Geologia, FACEN, Universidad Nacional de Asunción, San Lorenzo, Paraguay
[e] Laboratório de Geocronologia, Instituto de Geociências, Universidade de Brasília (UnB), s/n, CEP: 70919-970, Brasília, DF, Brazil
[f] Programa de Pós-Graduação em Geologia, Universidade de Brasília (UnB), Campus Universitário Darcy Ribeiro ICC, Asa Norte, CEP: 70919-970, Brasília, DF, Brazil

ARTICLE INFO

Keywords:
Caapucú suite
Paraguari belt
Brasiliano cycle
Petrology
Post-collisional magmatism
Western gondwana

ABSTRACT

The Caapucú Suite (CS), the focus of this study, includes Precambrian rocks that form the Alto Caapucú Block, located at the northern edge of the Rio de La Plata Craton in southern Paraguay. This is an acidic plutonic to volcanic magmatic suite, hosted in metavolcanic-sedimentary rocks of the Paso Pindó Group, which are in tectonic contact with the Villa Florida Metamorphic Suite of the Alto Caapucú Block. Based on the field and petrographic data of the CS, plutonic and volcanic lithotypes of this suite were identified, characterized and grouped into four petrographic facies: the rapakivi porphyritic syenogranite facies (RPSF), the monzogranite to alkali-feldspar microgranite facies (MAMF), the rhyolite facies (RF) and the ignimbrite facies (IF). These are underformed rocks of monzogranitic to syenogranitic composition with very-fine-to-medium grained crystals and inequigranular-to-porphyritic granophyric textures. The facies show circular-to-ring configurations with a large difference in relief in the area in which hypabyssal facies are partly surrounded by volcanic facies. The lithochemical analysis shows a limited compositional variation within this suite, which may be classified as acidic rocks, according to a silica content ranging from 73.9 to 79.2%. This corresponds to A-type granitoids that formed from metaluminous-to-slightly peraluminous ferrous magmatism in a post-collisional magmatic arc environment. The U—Pb (LA-ICPMS) geochronological data collected from zircon crystals suggest magma crystallization ages for the RPSF and IF of 563 ± 7.9 Ma and 565 ± 11 Ma, respectively. Based on these data, magmatism of the CS likely originated from Paraguari belt generated by agglutination of the Paranapanema and Rio de La Plata cratons. The CS presumably developed in the post-collisional stage of the Brasiliano/Pan-African Cycle during the formation of Western Gondwana. Considering the lithostratigraphic and structural framework of the CS, in addition to the collection of geochronological ages presented here and those previously available, the tectonic-magmatic correlation between the CS and the post-tectonic igneous events of the Ribeira and/or Dom Feliciano belts of the Mantiqueira Province is suggested.

1. Introduction

Precambrian rocks located in southern Paraguay termed the Alto Caapucú Block (Fulfaro and Palmieri, 1986), consists of a Paleoproterozoic crustal fragment and intrusions as well as a cover of Neoproterozoic metamorphosed supracrustal rocks.

The Paleoproterozoic basement is formed, according to Kanzler (1987), by the Villa Florida Metamorphic Suite, consisting of gneisses, amphibolites, quartzites, banded iron formation (BIFs) and phyllites. Neoproterozoic geological evolution is marked by the sin-colisional magmatism named Centu Cue Granodiorite, by occurrence of remnants of a low-grade metamorphic supracrustal sequence, the Paso Pindó

* Corresponding author. Programa de Pós-Graduação em Geociências, Universidade Federal de Mato Grosso (UFMT), Avenida Fernando Correa da Costa, s/n, CEP: 78.060-900, Cuiabá, MT, Brazil.
E-mail address: amandafgdleite@gmail.com (A.F. Granja Dorilêo Leite).

https://doi.org/10.1016/j.jsames.2018.09.016
Received 22 February 2018; Received in revised form 31 July 2018; Accepted 26 September 2018
Available online 15 October 2018
0895-9811/

Group, and by post-tectonic acid magmatism of the Caapucú Suite, which is the focus of this study (Chaney et al. 1982; Kanzler, 1987; Cubas et al. 1998; Meinhold et al. 2011).

Granitic magmatism is a key geological process related to the evolution of Brazilian orogens in the South American Platform. Magmatic batches associated with the evolution of these belts show that the magma production events that are responsible for building these orogens may be linked to pre-, syn-, late- and post-tectonic stages. These tectono-magmatic stages thus record different periods of the geodynamic evolution of Brazilian orogens. The post-collisional magmatism of the Brazilian Cycle in the mobile belts of the Mantiqueira Province has ages ranging from 650 to 580 Ma and is genetically linked to the development of large shear zones (Bitencourt and Nardi, 2000).

Considering that the Caapucú Suite is the largest granitic magmatic volume of the Alto Caapucú Block and that no robust geochronological data (such as U−Pb in zircon) or refined petrological data for this unit are available, this study uses field, petrographic, lithochemical and U−Pb geochronological data to contribute to the interpretation of tectonic and petrological evolution of this granitic suite and to define the age its associated magmatism.

Therefore, the Alto Caapucú Block plays an important role in the understanding of the geodynamic evolution of Western Gondwana, in particular the tectonic interactions between the Rio de la Plata and Paranapanema cratons and the Mantiqueira Province in southeastern Brazil.

2. Materials and methods

The petrographic analyses initially consisted of macroscopic studies, based on which samples were selected to prepare thin sections at the Laboratório de Laminação, of the Faculdade de Geociências (FAGEO), Federal University of Mato Grosso and were described in the Laboratório de Pesquisa of the same institution. In this study, 30 thin sections of all lithologies found in the area were described on the basis of texture, mineralogical composition and alteration processes, among other characteristics. Photomicrographs of thin sections were taken at 2.5, 4 and 10x magnification using a ZEISS camera coupled to an *Olympus* binocular optical microscope (model BX50). The abbreviations of Whitney and Evans (2010) were adopted to indicate the primary minerals in Figs. 4–7. Twelve samples were chosen for lithochemical analysis based on the petrographic descriptions.

The twelve most representative samples of the CS were selected for lithochemical analysis. Sample preparation for whole-rock chemical analyses (crushing, quartering and grinding to the 200-mesh fraction) took place at the *ALS Minerals* Laboratory (Goiânia – GO – Brazil). At this same laboratory, the samples (0.100 g) were digested to a lithium metaborate/tetraborate flux. The resulting melt is dissolved in 100 mL of 4% nitricacid/2% hydrochloric acid. Loss on ignition (LOI) was calculated using a prepared sample (1.0 g) which is placed in an oven at 1000 °C for 1 h, cooled and then weighed. The analyses were performed with an Inductively Coupled Plasma (ICP) technique to analyze major elements and an Inductively Coupled Plasma-Mass Spectrometry (ICP-MS) to analyze trace elements, including rare earth elements. The software GCDkit (version 2.3; Janousek et al., 2006) was used to process the data for petrogenetic interpretations. Geochemical data published by Cubas et al. (1998) were used for comparison to the data collected in this study, which were used in the diagrams proposed in gray fields.

The samples were initially prepared for geochronological analysis by disaggregation in a disk mill at the Laboratório de Preparação de Amostras of the Companhia Matrogrossense de Mineração (METAMAT). The grain concentrations were assessed according to conventional procedures for heavy minerals, including gravimetric and magnetic techniques, using the panning method and a Frantz magnetic separator at the Laboratório Intermediário de Geocronologia of FAGEO. Subsequently, approximately 100 zircon crystals of each sample were hand-picked under a binocular microscope.

U−Pb geochronological analyses by Laser Ablation-Inductively Coupled Plasma-Mass Spectrometry (LA-ICP-MS) were performed at the Geochronology Laboratory of the University of Brasília (UnB) and the procedures used followed the routine of Buhn et al. (2009). The equipment used for this analyses was the Neptune (Thermo-Finnigan) high-resolution multi-collector ICP-MS system coupled to an Nd-YAG (λ = 213 nm) Laser Ablation System (New Wave Research, USA). A mixture of Helium and Argon was used as a carrier gas. The laser frequency was 10 Hz, the energy was approximately 100 mJ/cm^2 and the spot size for U−Pb systematic analyses was approximately 30 µm. Plotting and regressions were performed using the algorithms and software Isoplot 3.0 developed by Ludwig (2003). All errors described in the diagrams, including the ellipsis error and calculated age, are based on the 2-σ level. Cathodoluminescence (CL) and back-scattered electron (BSE) microscopy images were taken with a scanning electron microscope to select the areas of analysis and to interpret the morphology of crystals.

3. Regional context

The Rio de La Plata Craton (RPC) is the oldest and southernmost Precambrian unit of South America and is considered to be the continental crust of the autochthonous Paleoproterozoic terrane in Southwestern Gondwana (Ramos et al., 1988; Rapela et al. 2007). The Paranapanema Block consists of a sequence of small, amalgamated cratonic fragments that stabilized during the formation of supercontinent Gondwana (Milani and Ramos, 1998; Padilha et al. 2015). These are covered by sediments of the Paraná Basin and are surrounded by Neoproterozoic belts (Cordani et al. 1984).

The Alto Caapucú Block is located between the Paranapanema and Rio de La Plata cratons, to the south of the Rio Apa Block and to the west of the mobile belts of the Mantiqueira Province, in southeastern Brazil (Fig. 1A). The basement rocks of the Alto Caapucú Precambrian Block, in southern Paraguay, are considered to be the an important exposure in the north of the RPC (Fulfaro, 1996; Rapela et al. 2007; Favetto et al. 2015).

Geophysical studies of Mantovani and Brito Neves (2005) indicate that the Alto Caapucú Block is slightly separated from the Paranapanema Block because its core is truncated by a marked lineament with an NW trend. Kanzler (1987) defined a NE-trending shear zone in the vicinity of Villa Florida, central-southern region of the Alto Caapucú Block, and considered that the tectonic structures originated in the Proterozoic, were reactivated during the Brasiliano Cycle and later in the Mesozoic (Drueker and Gay, 1985, in: Kanzler, 1987).

Almeida and Hasui (1984) and Cordani et al. (2001) considered that the NE-trending structures can be prolongations of those existing in Precambrian rocks of the Mantiqueira Province in southeastern Brazil (Fig. 1B). From geochronological data, Cordani et al. (2001) correlated the shear megazone close to Villa Florida to the Jacutinga megazone, which marks the limit of the Ribeira Belt with the Guaxupé Massif. The Maniqueira Province is a 3000 km long orogen that extends in NE-SW direction along the Atlantic coast of South America and is resulted from the Brasiliano/Pan-Africano convergence of cratonic blocks, leading to the amalgamation of the West Gondwana supercontinent.

The first contributions to the geological understanding of the rocks of southern Paraguay was a study by Harrington (1950), followed by studies of Eckel (1959), Putzer (1962) and Wiens (1984), who described and mapped the main Precambrian exposures. Kanzler (1987) used petrographic characteristics and outcrop exposures to establish the stratigraphic partitioning of the area.

According to Presser (1992), the Alto Caapucú Block can be considered a small Archean/Proterozoic cratonic block or microplate that constitutes a structural high characterized by an association of high-to medium-grade metamorphic rocks (gneisses, amphibolites, quartzites) and granitoids, besides volcanosedimentary rocks (Kanzler, 1987).

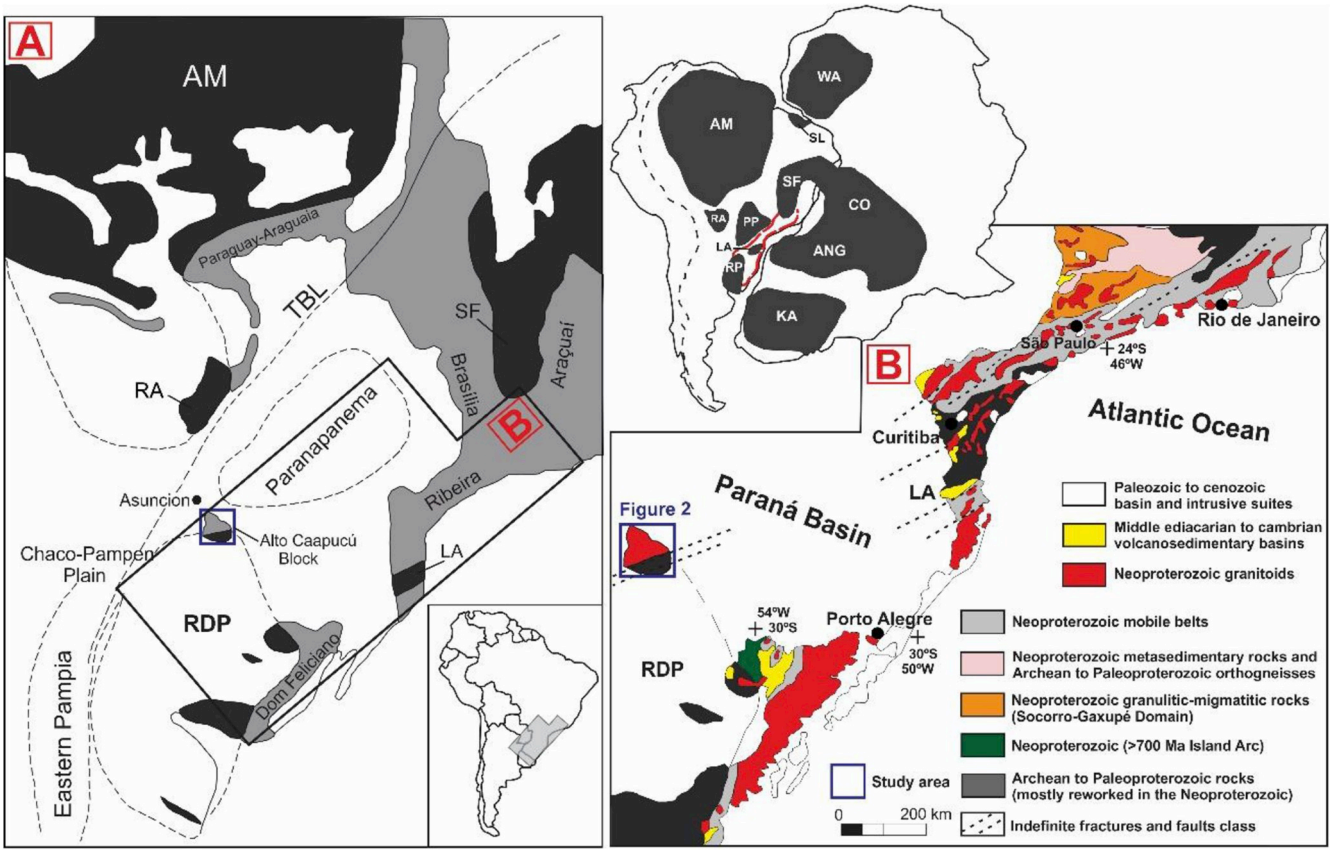

Fig. 1. A) geotectonic context of the southern region of the South American Platform and location of the region of study. Dotted lines indicate inferred boundaries of the main Precambrian crustal units. TBL = Trans Brazilian Lineament (modified from Rapela et al. 2007); B) geological context illustrating the NE tectonic trend and the units along the southern and central part of Mantiqueira Province (modified from Meira et al. 2015). AM – Amazonia Craton; ANG – Angola Block; CO - Congo Craton; KA – Kalahari Craton; LA - Luis Alves Craton; PP: Paranapanema Craton; RA – Rio Apa Block; RDP: Rio de La Plata Craton; SF: São Francisco Craton; SL – São Luis Craton; WA –West África Craton.

Cubas et al. (1998) presented the following stratigraphic subdivision for the rocks of this region: the Rio Tebicuary Complex, the Centu-Cue Granodiorite, the Passo Pindó Group and the Caapucú Suite. The first unit is composed of medium to high grade metamorphic rocks of the Villa Florida Metamorphic Suite. The Centu-Cue Granodiorite is associated with the basement and shows incipient foliation. The Passo Pindó Group is a metavolcanic-sedimentary unit that is discordant with the rocks of Rio Tebicuary Complex. The Caapucú Suite, the target of this study, intrudes all others (Fig. 2). The main data for these units are presented in Table 1.

The Villa Florida Metamorphic Suite, also named Complexo Rio Tebicuary by Wiens (1984), corresponds to rocks metamorphosed to the amphibolite to granulite facies, with evidence of partial anatexis, recorded in the granulites with segregation bands. The N70E-trending lineament pattern was described by Cubas et al. (1998) in these rocks, who also report closed and isoclinal folds with axes mainly trending NE-SW. Lohse (1990) performed the first geochronological analyses and obtained U–Pb ages in zircon between 2240 ± 20 Ma and 2040 ± 30 Ma.

Cubas et al. (1998) described the Centu-Cue Granodiorite as a coarse-grained, porphyritic to inequigranular batholith. The light-to dark-gray foliation follows the strike of the basement fault zone, indicating the syn-tectonic relationship of the granitic intrusion. K–Ar and Ar–Ar data for these rocks suggest a tectono-thermal event between 535 ± 30 Ma (Comte and Hasui, 1971) and 555 ± 9 Ma (Cubas et al. 1998).

According to Ruiz et al. (2018) an extensive neoproterozoic reworking is evidenced by superimposed tectonic structures, metamorphism and the K–Ar and Ar–Ar ages in Paso Pindó Group and Centu-Cue Suite. Ruiz et al. (2018) suggest the existence of Paraguari mobile belt, with N70-80E trend orogenic, composed by supracrustal rocks of Paso Pindó Group and a volumous granitic magmatisms of suítes Centu-Cue (0.62 Ga) and Caapucú (0.55 Ma), respectively.

The Caapucú Suite (CS) consists of an association of acidic plutonic and volcanic rocks and includes hypabyssal granites that are interspersed with tuffs and ignimbrites and are intruded by felsic dikes (Meinhold et al. 2011). The rocks occur as isotropic intrusions and the igneous outcrop at locations that are 120–180 km from the capital, Asunción.

Using data from Kanzler (1987), Cubas et al. (1998) identified four CS lithotypes based on crystal size, which they named according to the main sites of their occurrence: Barrerito, Casualidad, Charará and Fanego. In this study, a facies subdivision was chosen using a petrographic classification and following the criteria suggested by Ulbrich et al. (2001) and McPhie et al. (1993).

Cubas et al. (1998) suggested that the typological and textural differences found in these rocks result from distinct magmatic batches and crustal emplacement levels of this igneous event. These authors classify the magmatism as calc-alkaline, I-type series of a metaluminous-to-peraluminous character linked to a post-collisional continental arc environment.

Cordani et al. (2001) argue that the genesis of the rocks of Alto Caapucú block may be tectonically related to two regional events that affected the South American Platform: the Trans-Amazonian Cycle, which generated the rocks of the Rio Tebicuary Complex, and the Brazilian Cycle, which caused CS magmatism. The existing geochronological data for this suite are presented in Table 2.

The mobile belts from central-southern region of the Mantiqueira

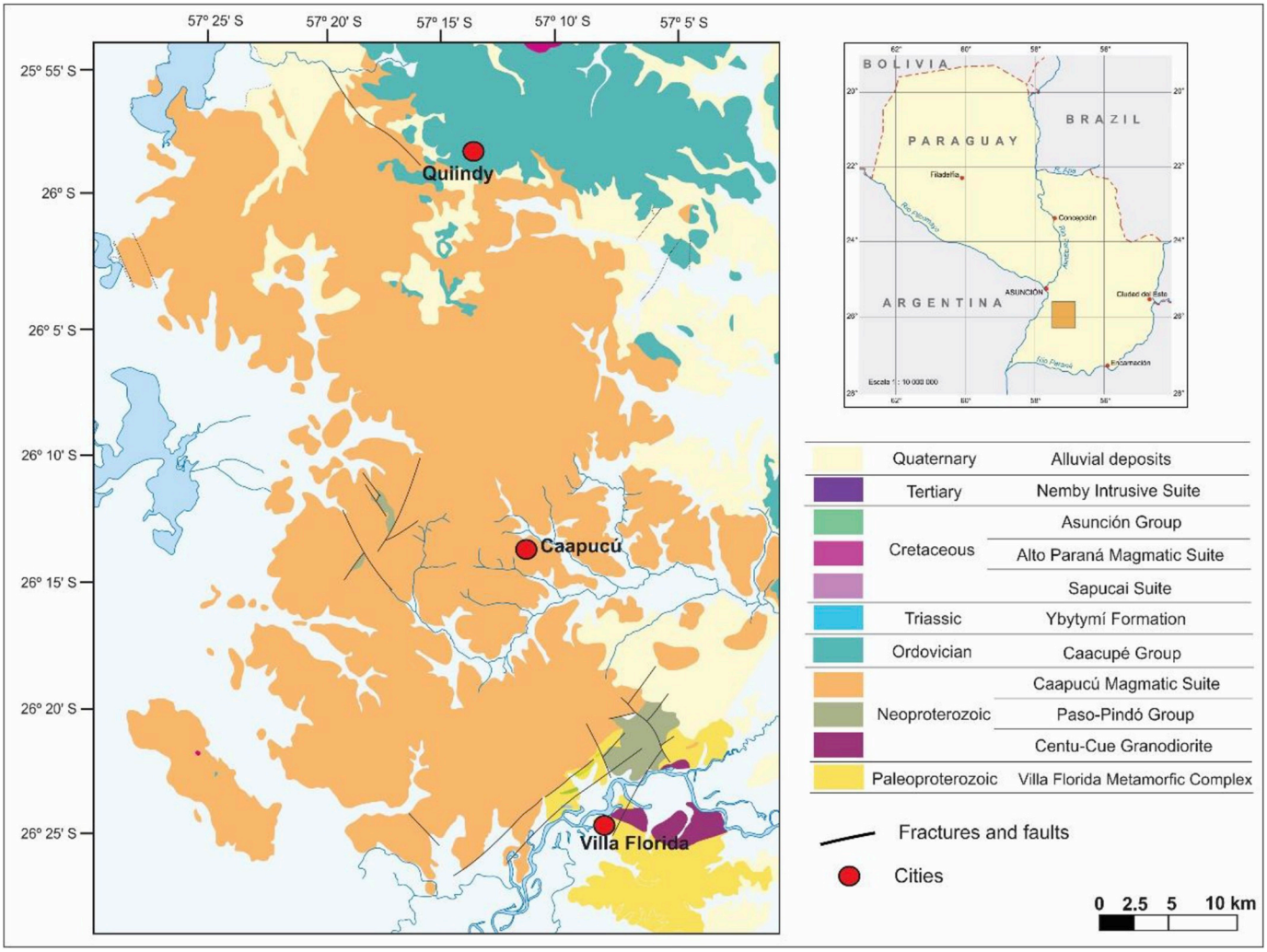

Fig. 2. Geologic Precambrian map of Alto Caapucú Block (Paula, 2018).

Table 1
Geological and geochronological summary data of Precambrian rocks in southern Paraguay.

Stratigraphic Unit	Reference	Method	Age (Ma)	Lithology
Caapucú Suite	Cordani et al. (2001)	Rb–Sr	560 ± 35	associations of acidic intrusive and extrusive rocks
Paso Pindó Group	Chaney et al. (1982)	–	–	metasediments (argillites, metasiltstones, metasandstones and metaconglomerates)
Centu-Cue Granodiorite	Cordani et al. (2001)	U–Pb	622 ± 15	white-to-gray granodiorite with a porphyritic texture
Villa Florida Metamorphic Suite	Cordani et al. (2001)	U–Pb	2023 ± 12	acidic, para- and ortho-gneisses, ferrous quartzite, marble and serpentinite

Table 2
Geochronological data available for the CS.

Authors	Method	Age (Ma)
Comte and Hasui (1971)	K–Ar	468 ± 25
Bitschene and Lippolt (1986)	Ar–Ar	544 ± 11
Cubas et al. (1998)	Rb–Sr	531 ± 5
Cordani et al. (2001)	Rb–Sr	560 ± 35

Province present their last phase of structuring intense post-collisional magmatic intrusions between 610 and 550 Ma in its last evolutionary phase (Meira et al. 2015; Phillipp et al., 2016). Some authors describe igneous suites very similar to those of CS as magmatic systems associated to remnant Braziliano mobile belt, such as those occurring in Mantiqueira Province, within Ribeira and Dom Feliciano belts systems (Table 3).

4. Results

4.1. Field and petrographic aspects

The rocks of the Caapucú Suite occur over an area of approximately 4000 km^2, from the city of Quindii to Villa Florida. They are mostly flooring outcrop rocks and isolated blocks with flat surfaces or can occur as small, aligned hills. They also occur in the margins of the Yparacaí Graben, near the cities of Paraguari and San Bernardino. The geological map of the area, originally reported by Cubas et al. (1998), was partly modified in this study.

Detailed study of the samples at macroscopic and microscopic scales enabled the differentiation of four facies variations based on differences in color, particle size, mineralogical composition and texture: the rapakivi porphyritic syenogranite facies (RPSF), the monzogranite to alkali-feldspar microgranite facies (MAMF), the rhyolite facies (RF) and the ignimbrite facies (IF; Table 4).

Table 3
Magmatism associated with the post-collisional period of the Brazilian/Pan-African cycle in the Ribeira and Dom Feliciano mobile belts.

Name of Magmatism/ Mobile belt	Reference	Age (Ma) and Geochronologic method	Characteristics
Pico do Parapagio Batholith/Ribeira	Meira et al. (2014)	579 ± 4 Ma (U–Pb)	granitic magmatism that includes metalunious batholits, peraluminous plutons and A-type granites. Syenogranites with inequigranular and hypdiomorphic textures.
Ubatuba Suite/Ribeira	Macluf and Schorscher (2001) Gasparini and Mantovani (1979)	~565 Ma 551 ± 5 Ma (Rb–Sr)	within-plate A-type leucogranites, with perthitic feldspar and equigranular to porphyritic textures.
Serra dos Órgãos Batholith/Ribeira	Tupinambá (1999)	559 ± 4 Ma (U–Pb)	megasheet of granodioritic to granitic orthogneiss emplaced during the syn- to late-collisional orogenic phase.
Suruí Granite/Ribeira	Valeriano et al. (2011)	511 ± 6.9 Ma (U–Pb)	elliptical puton of syenogranite porphyritic with K-feldspar as megacrysts. Pink-colored with fine-grained matrix.
Ilhabela Batholith/Ribeira	Barreto (2016)	~570 ± Ma	porphyritic granitoids with post-collisional A-type signature.
Dom Feliciano Suite/Dom Feliciano	Fragoso Cesar (1991)	550 ± 6 (Rb–Sr)	monzo- to syenogranites: pink-grayish porphyritic biotite-granites and coarse, reddish, equigranular, hololeucocratic granites.
Chasqueiro Granite/Dom Feliciano	Philipp et al. (2002a)	575 ± 8 (Pb–Pb)	monzo- to syenogranite, leucocratic of light-gray color and porphyritic texture with K-feldspar megacrysts in an equigranular matrix.
Ana Dias Rhyolite/Dom Feliciano	Oliveira (2015)	581.9 ± 2 (U–Pb)	porphyritic rhyolite and ignimbrites associated with granitic suites with fine particle size and affinity with the alkaline series.

Cartographic data from Cubas et al. (1998) show that the different facies of the CS have, into a two-dimensional view, circular and/or ring shapes (Fig. 3). The rocks do not show deformation, as the main tectonic stress, possibly originated in Phanerozoic, is essentially brittle.

The main relief difference in the area occurs because effusive volcanic rocks (rhyolite facies - RF) are found in regions of small hills and surrounded by plateaus in which intrusive facies outcrop (RPSF and MAMF). Criteria indicating the chronological relationship between facies could not be identified in the field. It was not possible to define the SC contact relations between the country rocks because there are no outcrops for this. Part of the area is covered by Phanerozoic sediments and there is no detailed cartography.

4.1.1. Rapakivi porphyritic syenogranite facies (RPSF)

The RPSF of the CS consists of rocks that mainly outcrop as small blocks and isolated boul with flattened surfaces. They are porphyritic leucocratic rocks, ranging from pink to grayish-pink (Fig. 4A and B), with a syenogranitic composition. They typically contain alkali feldspar phenocrysts covered by plagioclase, defining a rapakivi texture.

The rocks of this facies show an inequigranular to porphyritic texture with a xenomorphic matrix and a fine particle size. They essentially consist of quartz, perthitic to mesoperthitic alkali feldspars, plagioclase, biotite, aggregates of amphibole and alkali pyroxene (Fig. 4C). Zircon, apatite, titanite and opaque minerals are the accessory phases, whereas epidote/clinozoisite, sericite, clay minerals and chlorite are post-magmatic minerals.

The phenocrysts of these rocks have a particle size ranging from 1 to 4 mm, and they are represented by quartz, alkali feldspar and, more rarely, plagioclase. Optically, quartz crystals have a subhedral shape with particle size ranging from 0.3 mm to 3 mm. They are commonly found forming a granophyric texture with the perthitic orthoclase (Fig. 4D), with vermicular, cuneiform or lobed habits, mainly arranged on the edges of the feldspar.

Alkali feldspar crystals range from 0.1 to 4 mm and have a dusty appearance generated by clay formation/sericitization processes. The orthoclase crystals have subhedral shapes, may be covered by plagioclase and show perthitic to mesoperthitic intergrowths in which the sodic phase is arranged in threads, films and grains. The less abundant microcline ranges from 0.2 to 0.8 mm and is euhedral with *tartan* twinning.

Plagioclase (0.2–1 mm) occurs as tabular to anhedral crystals that are both aggregated and isolated and is classified, using the method by Michel Levy, as albite. Sporadically, plagioclase may involve alkali feldspar crystals forming a rapakivi texture (Fig. 4E). Plagioclase is usually zoned and clearly shows the effects of a saussuritization process (Fig. 4F).

Mafic minerals are arranged in aggregates formed by pyroxene, amphibole and biotite and opaque minerals (Fig. 4F).

Pyroxene, identified as of the aegirine-augite series, ranges from 0.1 to 0.3 mm and shows green-to-bluish-green pleochroism. Pyroxenes are sometimes zoned and partly replaced by fibrous amphibole, showing apatite and zircon inclusions (Fig. 4F). Furthermore, they may have a symplectitic texture.

Amphibole, identified as riebeckite, occurs as aggregates of subhedral crystals with sizes ranging from 0.1 to 0.6 mm, zoned from dark green in the core to brown in the edges, partly replaced by biotite. Some crystals show inclusions of tiny quartz grains.

Biotite (0.3–0.9 mm) is platy and anhedral with no preferential orientation, with a strong light-to-dark-brown pleochroism. Biotites crystals are often associated with amphibole (riebeckite) as its alteration product. Opaque minerals are usually anhedral and with sizes ranging from 0.1 to 0.3 mm.

4.1.2. Monzogranite to alkali-feldspar microgranite facies (MAMF)

MAMF is represented by subvolcanic rocks with equi-to-in-equigranular, xenomorphic-to-porphyritic, pink-to-pink-orangish

Table 4
Mineralogical and textural synthesis of the CS facies.

Facies	Primary mineralogy	Accessory mineralogy and mineral alteration	Textures
Rapakivi porphyritic syenogranite facies (RPSF)	quartz, alkali feldspars, plagioclase, biotite and alkali amphibole and pyroxene	zircon, apatite, titanite, opaque minerals, epidote, sericite, clay minerals and chlorite	porphyritic, perthitic, graphic and rapakivi
Monzogranite to alkali-feldspar microgranite facies (MAMF)	quartz, alkali feldspars, plagioclase, biotite, hornblende	zircon, apatite, opaque minerals, muscovite, epidote, sericite and chlorite	porphyritic, perthitic and graphic
Rhyolite facies (RF)	quartz, alkali feldspar, plagioclase and biotite	zircon, opaque minerals, titanite, apatite, epidote clay minerals, and chlorite	porphyritic and glomeroporphyritic
Ignimbrite facies (IF)	quartz, alkali feldspar, plagioclase and biotite	apatite, zircon, opaque minerals, chlorite, clay minerals and chlorite	eutaxitic and micropoikilitic

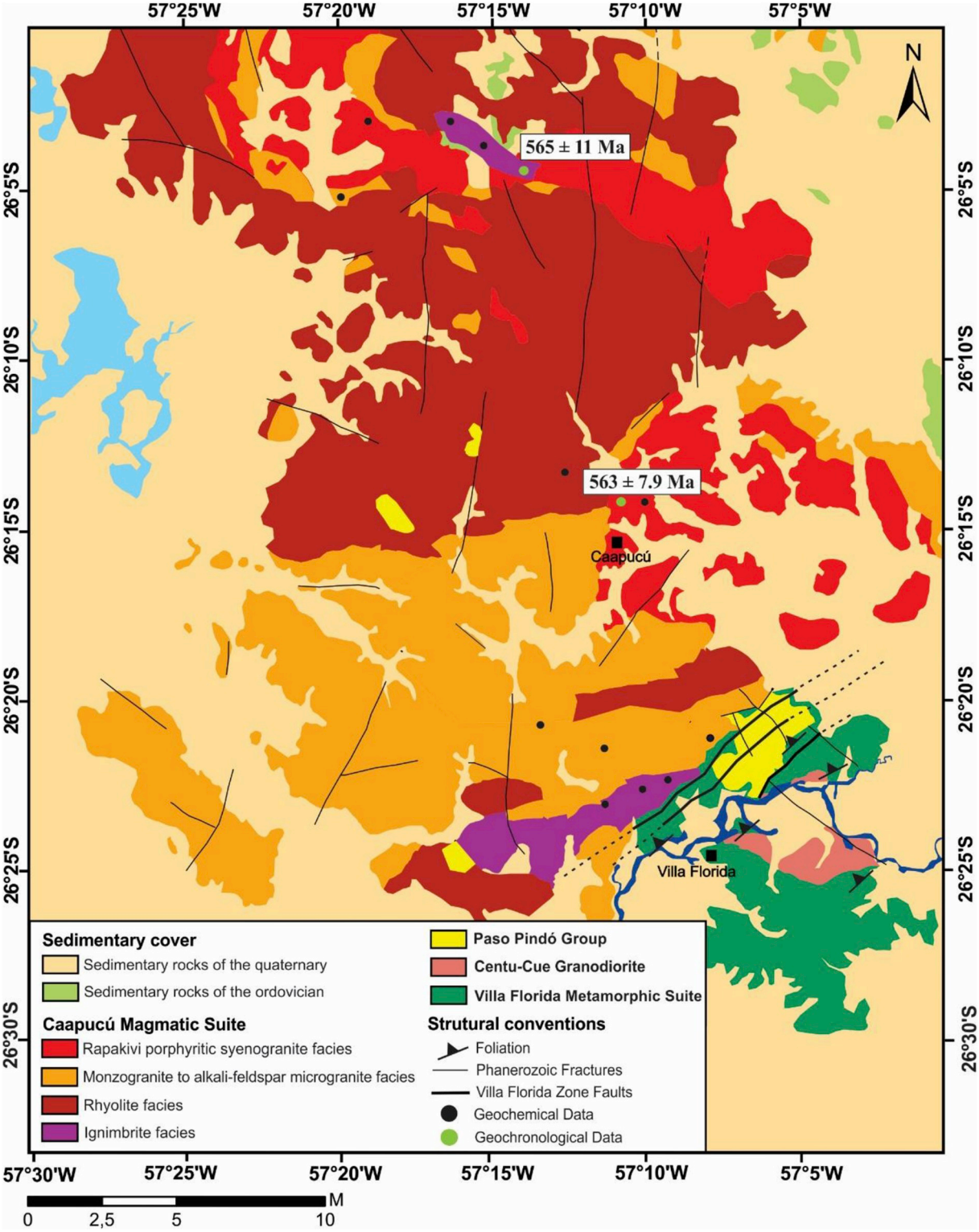

Fig. 3. Geological map of the Caapucú Suite with location of geochronological U–Pb and geochemical samples (modified from Cubas et al. 1998).

textures (Fig. 5A, C and 5E), which outcrop as blocks, boulders and slab rocks in flattened regions. The percentage of mafic mineral is lower than 5%, providing them a hololeucocratic character. The composition is mostly quartz and feldspar associated with a finer grained groundmass, which enables the differentiation from the previous facies. A clear variation in particle size among these lithotypes, ranging from very fine to medium, is highlighted.

This facies essentially consists of quartz crystals, alkali feldspars, plagioclase, rare biotite and minor hornblende. Zircon, apatite and opaque minerals represent the accessory paragenesis. Muscovite, sericite, chlorite, clay minerals and epidote are products of post-magmatic alteration.

When the rocks have porphyritic textures, the matrix has a quartz-feldspar composition with very fine- (Fig. 5B) -to-fine (Fig. 5D) particle sizes. Phenocrysts range from 1 to 3 mm and consist of quartz and alkali feldspar. Rocks with fine particle size and equigranular texture

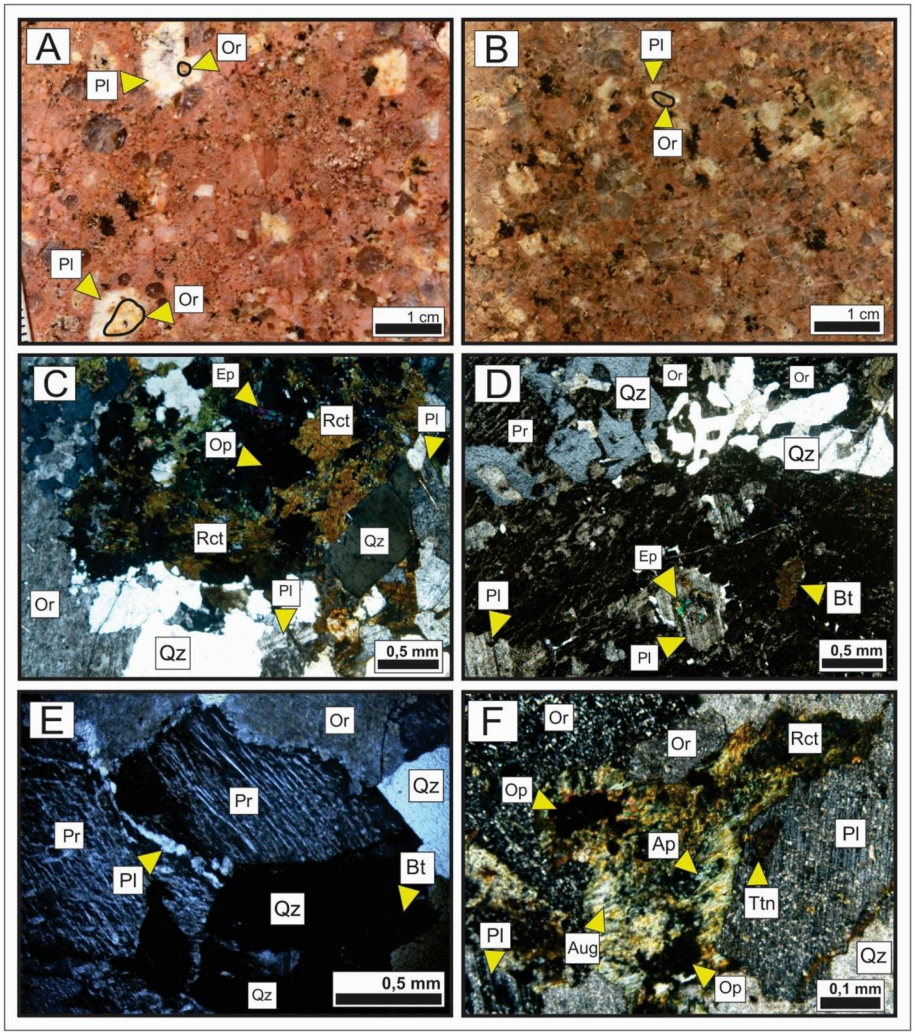

Fig. 4. Characteristics of the RPSF of the CS: A) and B) pink and grayish-pink hand samples, respectively, both with rapakivi texture; C) photomicrograph showing inequigranular, xenomorphic texture formed by perthitic alkali feldspar, plagioclase, quartz and aggregates of amphibole and opaque rocks, and microgranular biotite; D) detailed photomicrograph showing perthite in the middle of a granophyric texture, with grains of zoned plagioclase and epidote from saussuritization; E) photomicrograph showing a rapakivi texture; F) photomicrograph of saussuritized plagioclase crystals and of pyroxene altered to fibrous amphibole, apatite and titanite. Images C to F were taken under crossed polarizers. Pr: Perthite. (For interpretation of the references to color in this figure legend, the reader is referred to the Web version of this article.)

sporadically occur, and higher quantities of plagioclase (29%) classify them as monzogranites (Fig. 5F).

Quartz has a subhedral habit or a vermicular shape, forming granophyric intergrowth. Quartz is found in the matrix and as phenocrysts, which range from 0.5 to 3 mm, showing bight and corrosion gulfs. In isolated points of the matrix, quartz may show aggregates of very fine particles.

Alkali feldspar usually occurs as grains ranging from subhedral to anhedral and is represented by the orthoclase with Carlsbad twinning (Fig. 5D). When in phenocrysts, alkali feldspar has a particle size ranging from 0.1 to 2 mm, is anhedral and show stringers and drops perthites to mesoperthites (Fig. 5B), granophyric intergrowth and dusty aspect due to the effects of argilization and sericitization.

Plagioclase crystals range from subhedral to anhedral, with sizes ranging from 0.4 to 2 mm and show albite- and pericline-type polysynthetic twinning (Fig. 5F). Plagioclase is argilized or saussuritized and shows normal zonation, evidenced by cores that are more altered than edges.

Biotite has a particle size ranging from 0.2 to 0.9 mm and occurs at a percentage lower than 5%. Biotite shows a micaceous habit and light-to-dark-brown pleochroism without preferential orientation. Amphibole that has partly been altered to platy biotite sporadically occurs.

Muscovite is a secondary phase and occurs as very-fine-to-fine plates, which commonly include opaque minerals. Sericite occurs as a set of minute crystals arranged in bands.

Epidote (allanite) forms very fine euhedral grains, which can be found in longitudinal sections that correspond to well-developed prisms.

4.1.3. Rhyolite facies (RF)

RF includes gray leucocratic rocks (Fig. 6A) with porphyritic textures in an aphanitic matrix, which mainly occur as blocks and boulders near roads. RF is intersected by dykes that are slightly thicker than 1 cm (Fig. 6B) and composed by very fine syenogranitic rock related to the monzogranite to alkali-feldspar microgranite facies (MAMF).

Optically, RF typically has a porphyritic texture, sometimes glomeroporphyritic, and a very fine quartz-feldspathic matrix that consists of quartz, alkali feldspar, plagioclase and biotite, whereas zircon, opaque minerals, titanite and apatite represent accessory paragenesis, and clay minerals, epidote and chlorite occur as post-magmatic products. Anhedral lithoclasts (less than 5%) formed by quartz, alkali feldspar, plagioclase, biotite, titanite, opaque minerals, apatite and epidote are more than 0.1 mm in size (Fig. 6C). The lithoclasts are cognate of the rhyolitic rocks, representing portions of the same magma.

Quartz occurs as a mesostatic component or as anhedral phenocrysts up to 2 mm, showing intense magmatic corrosion and bight. Quartz is also found in recrystallized phase.

Feldspar phenocrysts range from 1 to 2.5 mm and are commonly sericitized, argilized or saussuritized producing secondary paragenesis formed by sericite, clay minerals, carbonate and minerals of the epidote group. Alkali feldspar is represented by orthoclase with Carlsbad twinning (Fig. 6D) and with evidence of exsolution as a stringers and

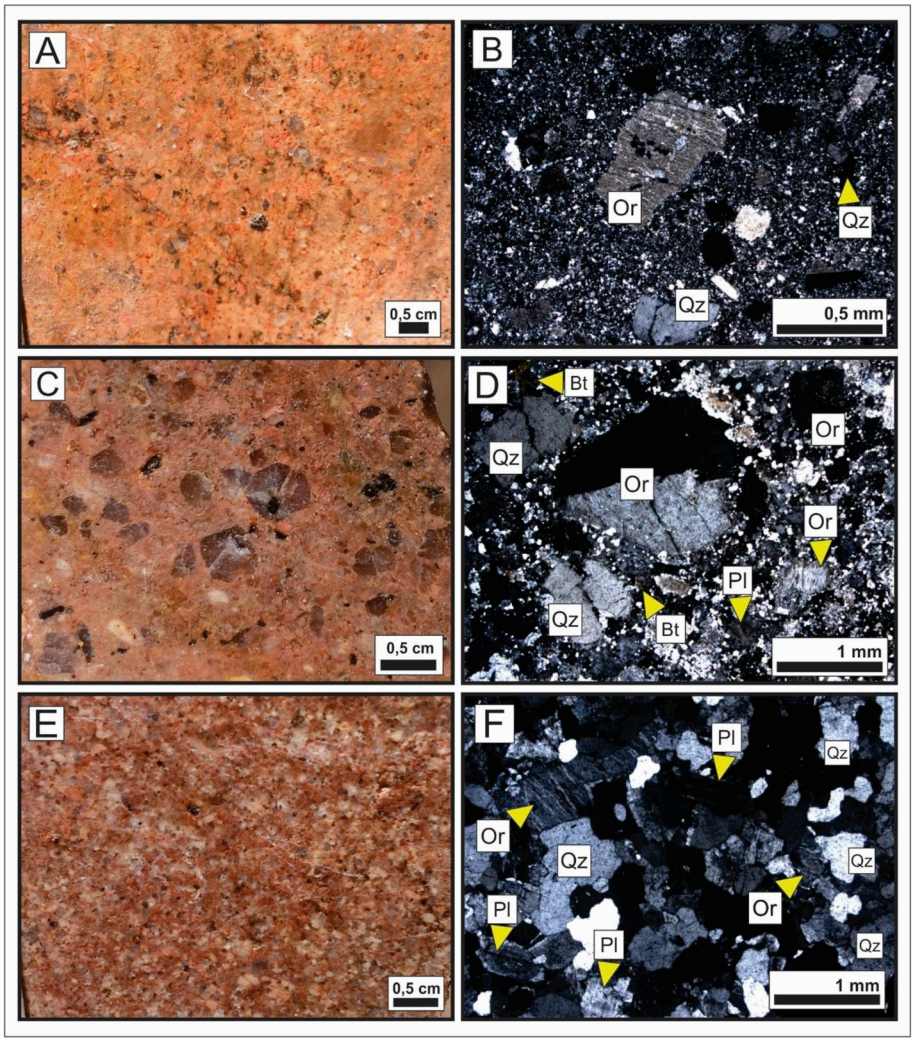

Fig. 5. Characteristics of the MAMF of the CS: A), C) and E) hand samples of pink-to-pink-orange porphyritic rocks of different particle sizes; B) photomicrographs showing phenocrysts of argilized perthitic feldspar and quartz in a very fine quartz-feldspathic matrix; D) photomicrographs showing a porphyritic texture formed by orthoclase phenocrysts with Carlsbad twinning in a fine matrix; F) photomicrograph showing xenomorphic equigranular texture formed by perthitic alkali feldspars, quartz and rare plagioclase. Images B, D, and F were taken under crossed polarizers. (For interpretation of the references to color in this figure legend, the reader is referred to the Web version of this article.)

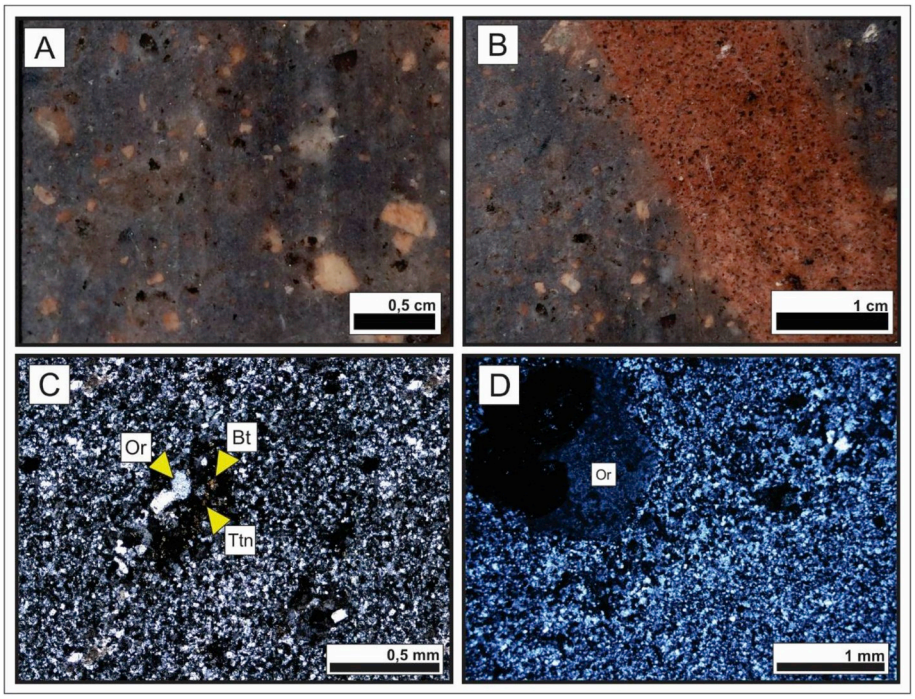

Fig. 6. Characteristics of the RF of the CS: A) hand sample showing a porphyritic texture with alkali feldspar phenocrysts, quartz and mafic aggregate in a very fine, gray matrix; B) hand sample showing contact between the RF and the syenogranitic dyke of the MAMF; C) photomicrograph showing a lithoclast consisting of quartz, alkali feldspar, plagioclase, biotite, epidote, titanite, opaque minerals and apatite; D) photomicrograph showing an alkali feldspar phenocryst with Carlsbad twinning in a very fine felsitic matrix. Images C and D were taken under crossed polarizers.

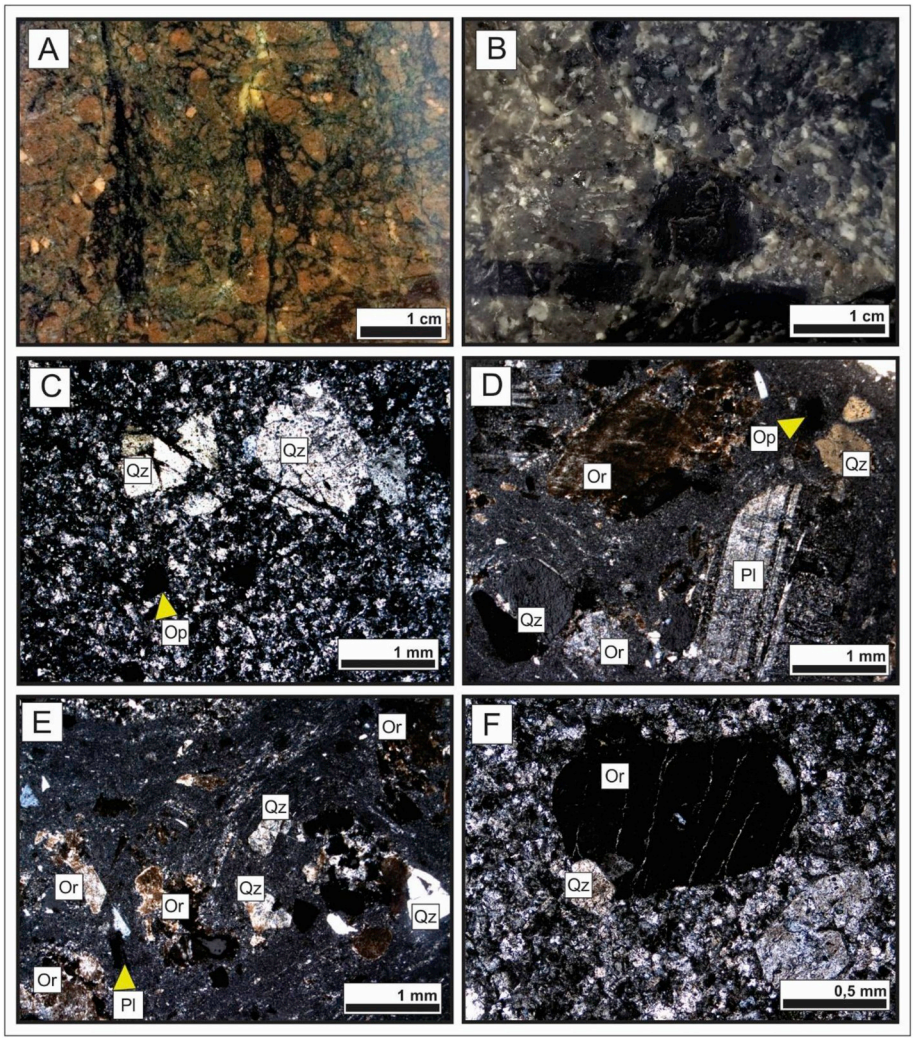

Fig. 7. Petrographic characteristics of the IF of the CS: A) reddish-brown hand sample showing an aphanitic matrix; B) gray hand sample with rounded and elongated black lithic fragments with centimeter-scale dimensions. The matrix shows an aphanitic texture; C) photomicrograph showing angular, fractured and corroded crystalloclasts in the middle of a devitrified matrix with an micropikilitic texture; D) photomicrograph showing plagioclase crystalloclasts, alkali feldspar and quartz in the middle of a matrix with very fine, gray particles; E) photomicrograph showing the alignment of fiammes in planar foliation; F) photomicrograph with the detail of a rounded perthitic alkali feldspar crystalloclast in a matrix with an micropikilitic texture. Images C to F were taken under crossed polarizers. (For interpretation of the references to color in this figure legend, the reader is referred to the Web version of this article.)

drops perthites textures.

Biotite occurs at a percentage lower than 5% in small plates, with light-to-dark-brown pleochroism, and can be partly-to-totally chloritized.

Opaque minerals range from 0.1 to 0.3 mm and may occur in the matrix or as inclusions in phenocrysts and in lithoclasts. They have euhedral shapes and commonly show a rim of reaction to titanite and symplectite-to-poikilitic texture.

4.1.4. *Ignimbrite facies (IF)*

The acid pyroclastic rocks of the CS occur in the northern and southern regions of the study area and were genetically classified as ignimbrites with a rhyolitic composition. They feature a massive structure and colors ranging from reddish brown to gray (Fig. 7A and B). Furthermore, they contain feldspar and quartz phenocrysts in an aphanitic matrix.

Optically, the IF includes crystal-rich, gray, fine-to-very-fine rocks with felsitic mesostasis and some lithic fragments. Occasionally, the matrix is devitrified, showing an initial stage of nucleation and mineral neoformation due to thermodynamic instability of the glassy portions. Micropoikilitic texture is developed as a product of devitrification and consists of an irregular mosaic intergrowth of anhedral quartz and feldspar crystals (Fig. 7C and F).

Crystalloclasts exhibit angular, fractured and corroded features (Fig. 7C) with sizes ranging from 0.4 to 4 mm, predominantly consisting of quartz and alkali feldspar with subordinate amount of plagioclase (Fig. 7D). The accessory mineralogy is represented by biotite, apatite, zircon and opaque minerals, whereas chlorite and clay minerals correspond to the alteration minerals.

The lithic fragments have rounded and elongated shapes with centimeter-scale dimensions (Fig. 7B). Under the microscope, these fragments from 5 mm in size can represent two types of genesis: cognate terms of rocks of similar composition, characterizing portions of the same magma, and non-cognate terms, corresponding to accidental lithic clasts. The lithoclasts can represent the beginning of the volcanic phase, with the opening of the volcanic conduit.

The welding process promotes the development and alignment of the fiammes in a planar foliation due to the parallel arrangement of flattened fragments, termed a eutaxitic texture (Fig. 7E). Fiammes usually surround crystalloclasts glassy lenses with flame-like shapes.

Quartz occurs as subhedral grains, usually fractured and with sizes ranging from 0.4 to 4 mm. Quartz is a very common phase and shows bight and corrosion gulf structures.

Alkali feldspars are usually argilized with particle sizes ranging from 0.8 to 3 mm and round, subhedral-to-anhedral shapes. They include orthoclase with Carlsbad twinning and microcline, to a lesser extent, with tartan twinning. Orthoclase crystals show a perthitic texture in stringers and in drops (Fig. 7F) and corrosion gulfs.

Plagioclase is rarer and has a tabular shape and euhedral habit with sizes ranging from 0.4 to 1 mm, showing polysynthetic twinning and incipient saussuritization.

Opaque minerals have subhedral-to-anhedral habit consisting of very fine grains; they are very commonly surrounded by microgranular chlorite.

Table 5
Results of CS chemical analysis.

Elements	RPSF ▲		MAMF ▲				RF ▲	IF ▲				
	AG04	AG10	AG05	AG08	AG12	AG13	AG02	AG06	AG07	AG14	AG15-1	AG15-2
SiO_2	78,2	74,9	77,3	78,5	78,1	75,8	73,9	75,9	76,2	79,2	75,5	76,1
Al_2O_3	12,75	13,2	11,6	11,75	11,65	12,45	12,75	11,85	11,65	10,7	12,5	12,6
Fe_2O_3	1,93	2,28	1,94	2,51	1,35	2,06	1,93	1,95	2,13	2,67	3,13	3,32
MnO	0,03	0,07	0,03	0,03	0,02	0,05	0,03	0,05	0,04	0,03	0,07	0,06
MgO	0,08	0,27	0,01	0,12	0,02	0,21	0,29	0,19	0,29	0,14	0,18	0,28
CaO	0,37	0,94	0,35	0,34	0,2	0,65	0,9	0,63	0,77	0,18	1,45	1,31
Na_2O	3,15	3,68	3,14	3,22	3,27	3,48	3,93	3,18	3,13	2,16	3,71	3,57
K_2O	5,2	4,71	4,73	4,85	4,68	4,7	4,42	4,69	4,72	5,11	3,34	3,59
TiO_2	0,18	0,21	0,07	0,17	0,09	0,23	0,26	0,18	0,12	0,2	0,22	0,24
P_2O_5	< 0,01	0,05	< 0,01	0,33	< 0,01	0,04	0,03	0,02	0,01	< 0,01	0,03	0,03
LOI	0,25	0,38	0,38	0,32	0,41	0,41	0,31	0,43	0,8	0,65	0,47	0,6
Total	101,66	100,78	99,59	101,89	99,81	100,19	98,93	99,18	99,94	101,08	100,67	101,78
Ba	503	702	290	368	69,6	832	1555	803	532	139,5	430	0,05
Co	1	3	1	1	2	2	1	2	2	< 1	1	2
Cs	4,55	4,96	0,94	3,6	5,85	2,76	1,78	2,27	1,51	0,65	6,13	3,29
Ga	20,3	19,2	19,5	19,1	19,7	22,6	17,9	21,2	20	29,4	22,6	22,8
Hf	6,6	4,5	6,5	5,1	4,1	6,4	7,4	5,2	4,2	24,3	7,4	7,2
Nb	18	10,1	20,1	15,9	17,8	13,4	16	17,3	13	49	13,4	13,4
Rb	224	162	188	195	267	151	135,5	155	159,5	132,5	146,5	161
Sr	49,7	106,5	41,2	53,3	22	100,5	98,7	79,7	48,9	69,4	123,5	130,5
Ta	1,5	0,8	1,3	1,4	1,8	1	1,1	1,4	1,2	2,8	1,2	1,3
Th	24,7	24,4	20,3	27,1	34,1	20,1	18,15	16,55	18,05	18,1	12,8	14,15
U	4,34	3,99	1,58	5,06	3,73	3,56	3,67	2,79	3,07	2,54	4,09	4,27
W	6	6	5	2	4	2	15	2	3	1	3	6
Zr	217	148	165	152	95	225	269	175	121	1080	304	272
Y	37,8	21	31,5	35,4	27,1	29,4	35,1	33,8	34,7	110	47,4	48,1
La	52,7	33,5	6,7	43,7	10,6	48,7	73,2	56,2	52	120	35,2	36,1
Ce	86,7	63,9	61,2	82	34,8	102,5	136	109,5	97,2	238	73,9	74,7
Pr	10,85	6,6	1,87	8,88	2,74	10,75	14,85	11,6	10,5	27,6	8,61	8,94
Nd	36,9	22,6	7,5	29,4	9,1	40	52,3	39,8	35,7	102	34,5	36,3
Tm	0,72	0,38	0,68	0,53	0,51	0,45	0,56	0,53	0,57	1,59	0,74	0,68
Sm	6,53	4,03	2,06	6,01	2,45	6,73	8,63	6,85	5,93	19,25	7,2	7,72
Eu	0,78	0,68	0,31	0,46	0,18	1,18	1,3	0,91	0,52	0,33	1,38	1,52
Gd	5,64	3,35	3,39	4,95	2,69	5,44	7,04	5,79	5,13	19,05	7,55	7,74
Tb	0,98	0,56	0,62	0,85	0,54	0,86	1,06	0,95	0,93	3,09	1,29	1,34
Dy	5,94	3,19	4,27	4,58	3,57	4,98	5,59	5,57	5,33	18,45	7,25	7,62
Ho	1,34	0,66	1,11	1,13	0,83	1,02	1,2	1,11	1,12	3,8	1,69	1,62
Er	4,2	2,08	3,94	3,31	2,99	3,05	3,59	3,53	3,64	10,85	4,92	4,89
Yb	4,91	2,49	4,92	3,96	3,71	3,22	3,58	3,49	3,96	10,95	5,05	4,95
Lu	0,81	0,41	0,74	0,65	0,65	0,54	0,53	0,55	0,61	1,55	0,73	0,74
Eu/Eu*	0,39	0,55	0,36	0,25	0,21	0,58	0,50	0,43	0,28	0,05	0,57	0,60
$(La/Yb)_N$	7,18	9,00	0,91	7,38	1,91	10,11	13,67	10,77	8,78	7,33	4,66	4,88

Biotite shows particle sizes ranging from 0.3 to 0.5 mm in anhedral plates and is commonly associated with opaque minerals. Biotite is also found in lithic fragments as aggregates with quartz, feldspars, epidote, chlorite and clay minerals.

4.2. CS lithochemistry

Chemical analysis of the CS rocks show narrow compositional variation. These rocks are classified as acidic, with silica content ranging from 73.9 to 79.2%. Data for major and trace elements are presented in Table 5. The findings were plotted in diagrams commonly used in the literature in which the data for the CS rocks published by Cubas et al. (1998) are also plotted in gray fields.

The CS volcanic rocks are geochemically classified as rhyolite and alkali rhyolite, and the plutonic rocks as granite to alkali granite, according to the R1-R2 diagram proposed by La Roche et al. (1980), illustrated in Fig. 8A and B, respectively. The normative composition shown in the Ab-An-Or diagram by O'Connor (1965; Fig. 8C) shows a granitic composition for the plutonic samples.

The FeOtot/(FeOtot + MgO) *versus* SiO_2 diagram proposed by Frost et al. (2001; Fig. 9A), as well as the A/CNK *versus* A/NK diagrams proposed by Maniar and Picolli (1989; Fig. 9B), based on Shand indices, suggest that the CS rocks originated from a ferrous and metaluminous-to-slightly peraluminous signature. In the first diagram (Fig. 9A), there is a boundary separating the two fields because suites with A-type characteristics are distinctly more iron enriched than the Cordilleran-type granitoids (Frost and Frost, 1997). The CS samples plot in the ferroan field and can be named A-type granitoids (Frost et al. 2001).

The CS analytical data, when plotted in the Harker (1909) diagrams, which show major elements as a function of silica content (Fig. 10), indicate negative correlations between this index and Al_2O_3, CaO and Na_2O, suggesting mainly plagioclase fractionation. TiO_2, FeOt, MgO, K_2O and P_2O_5 show dispersion patterns, which may indicate crustal contamination or later modifications that may have resulted from hydrothermal processes, for example. In two samples of the IF, occur a relative enrichment in CaO, FeOt and MgO contents that possibly is associated with the presence of lithic fragments with greater amount of chlorite and clay minerals, described in petrography. These same samples are K_2O depleted which suggests a relative decrease of porphyroclastic of alkali feldspar.

The distribution of trace elements in the Harker (1909) diagrams indicates a positive correlation between the differentiation index (silica) and Rb, whose content ranges from 120 to 280 ppm, indicating the enrichment in alkali feldspar of the most evolved rocks. Sr and Ba are negatively correlated with SiO_2, suggesting feldspar fractionation and a high magma differentiation rate (Vavra, 1994). The IF comprises several amount of lithic fragments and crystalloclasts and the analytical data are influenced by them. Thus, some samples of this facies present

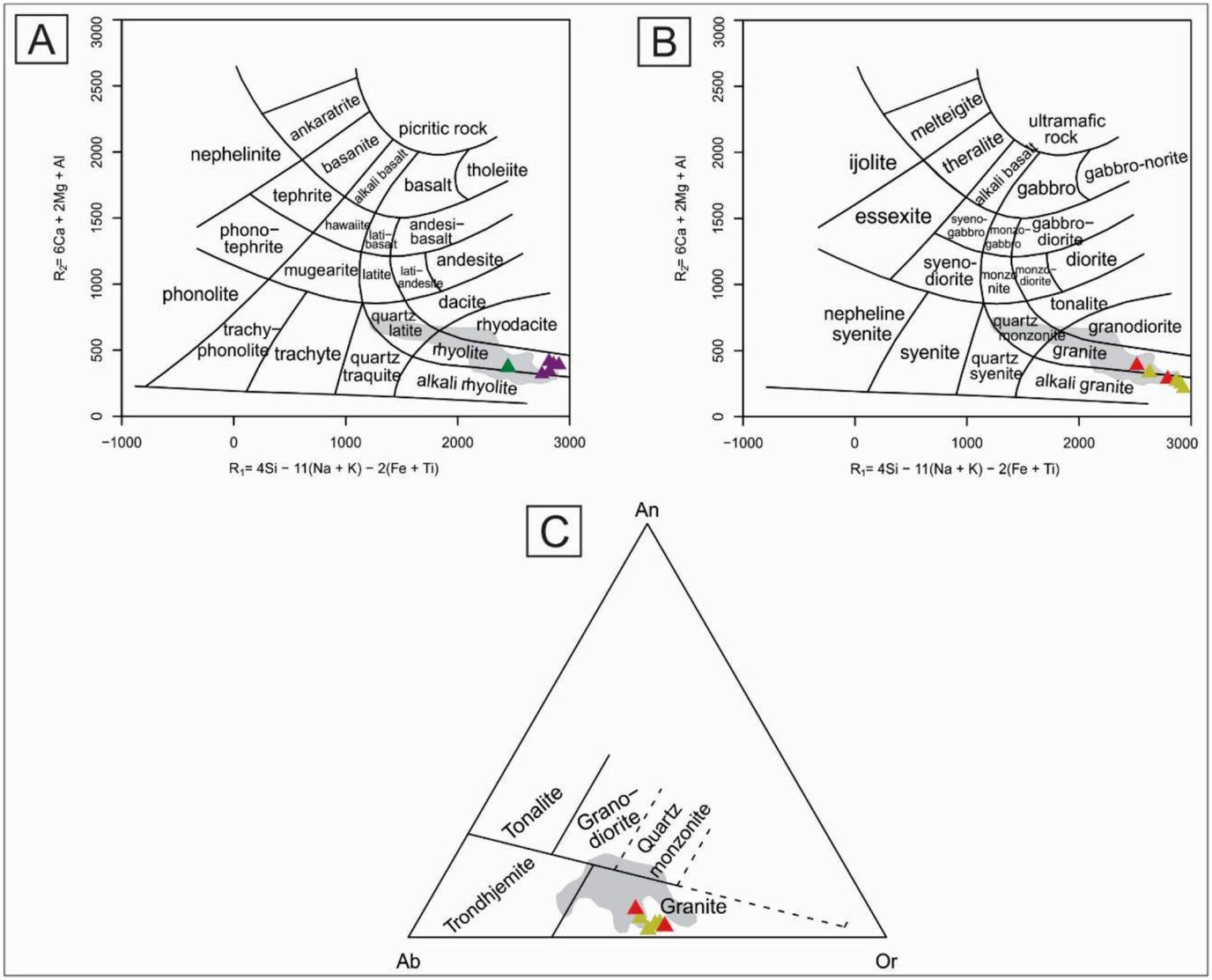

Fig. 8. Distribution of data of representing CS rocks in the following diagrams: (A) R1-R2 proposed by La Roche et al. (1980) for volcanic samples; (B) R1-R2 proposed by La Roche et al. (1980) for plutonic samples and (C) Ab-An-Or normative molecular composition, according to the parameters by O'Connor (1965). Gray fields: CS geochemical data published by Cubas et al. (1998).

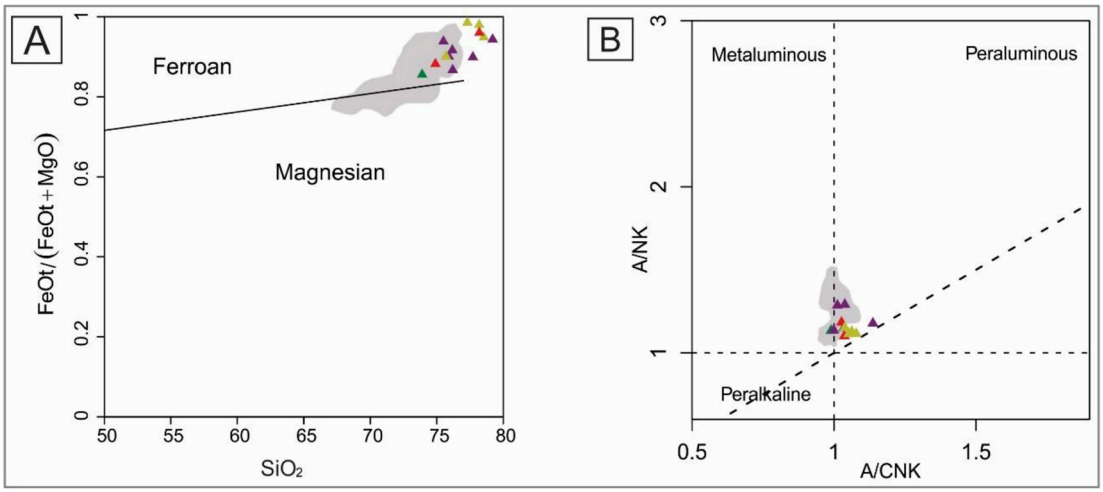

Fig. 9. Distribution of data of representing CS rocks in the following diagrams: (A) FeOtot/(FeOtot + MgO) *versus* SiO_2 diagram, proposed by Frost et al. (2001), and (B) A/CNK *versus* A/NK diagram by Maniar and Picolli (1989). Gray fields: CS geochemical data published by Cubas et al. (1998).

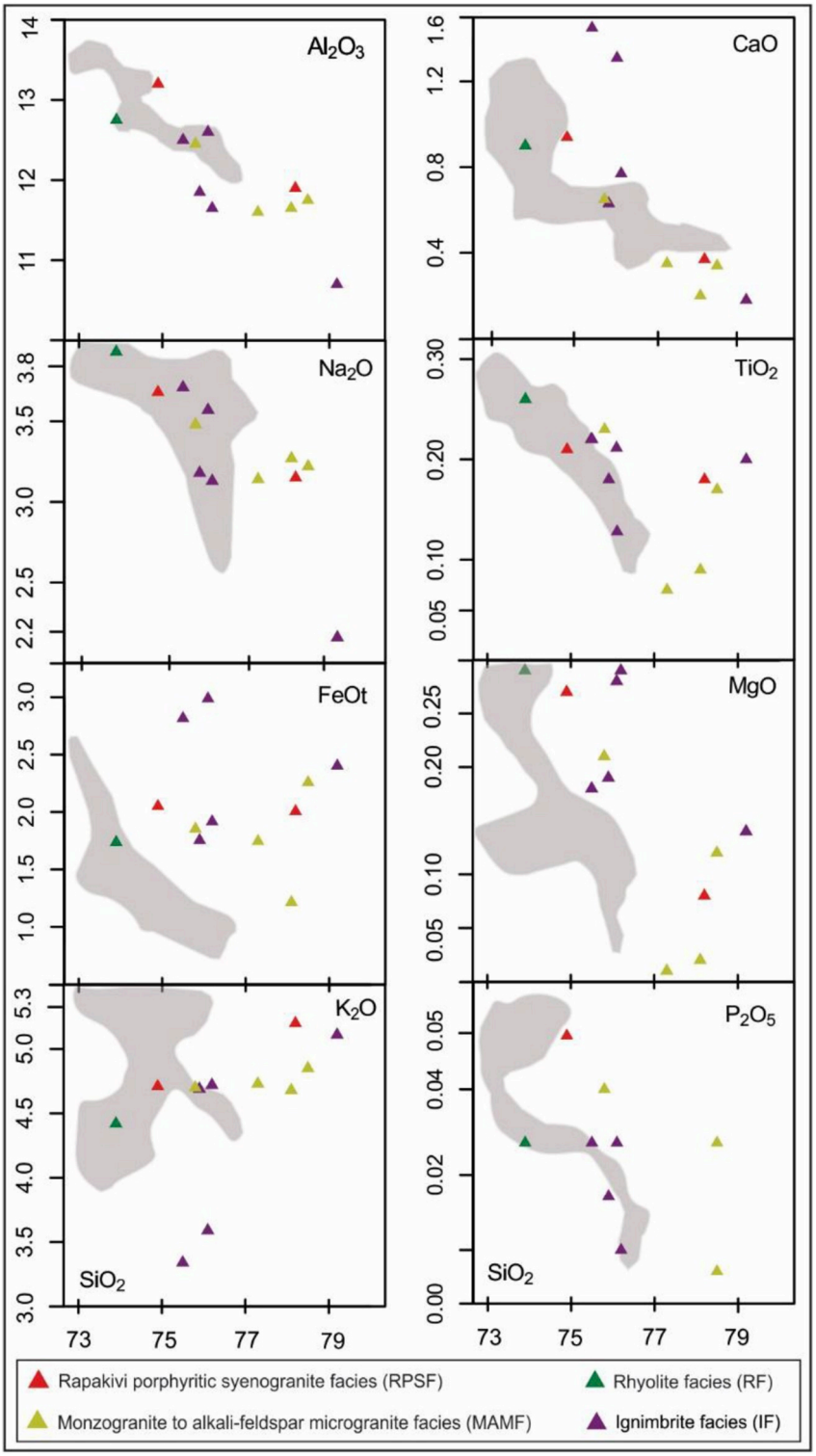

Fig. 10. Harker (1909) diagram with the distribution of data of major elements expressed in oxides of CS rocks. Gray fields: CS geochemical data published by Cubas et al. (1998).

enrichment of Ce, Y and Sr that could be related to a greater amount of modal epidote, apatite and phenocrysts of plagioclase, respectively. Moreover, the high Zr contents in one sample indicate abundance of zircon in this rock (Fig. 11).

The CS rare earth elements (REE) data, normalized using the chondritic values of Nakamura (1974; Fig. 12), mostly show a fractionation pattern of heavy REE relative to light REE. The $(La/Yb)_n$ ratios ranged from 0.91 to 13.67 in MAMF and RF rocks, respectively, whereas the heavy REE showed a subhorizontal pattern generating a configuration similar to the shape of a seagull's wing (Fig. 12), which characterizes an alkaline series. The higher REE contents in the IF sample (Fig. 12A) results from the proportional enrichment of these elements in relation to the gain or loss of more mobile ones in post-crystallization processes, such as hydrothermalism and/or metasomatism (Liaghat and MacLean, 1995). The MAMF samples (Fig. 12B) presents two light REE patterns, one with higher and one with lower

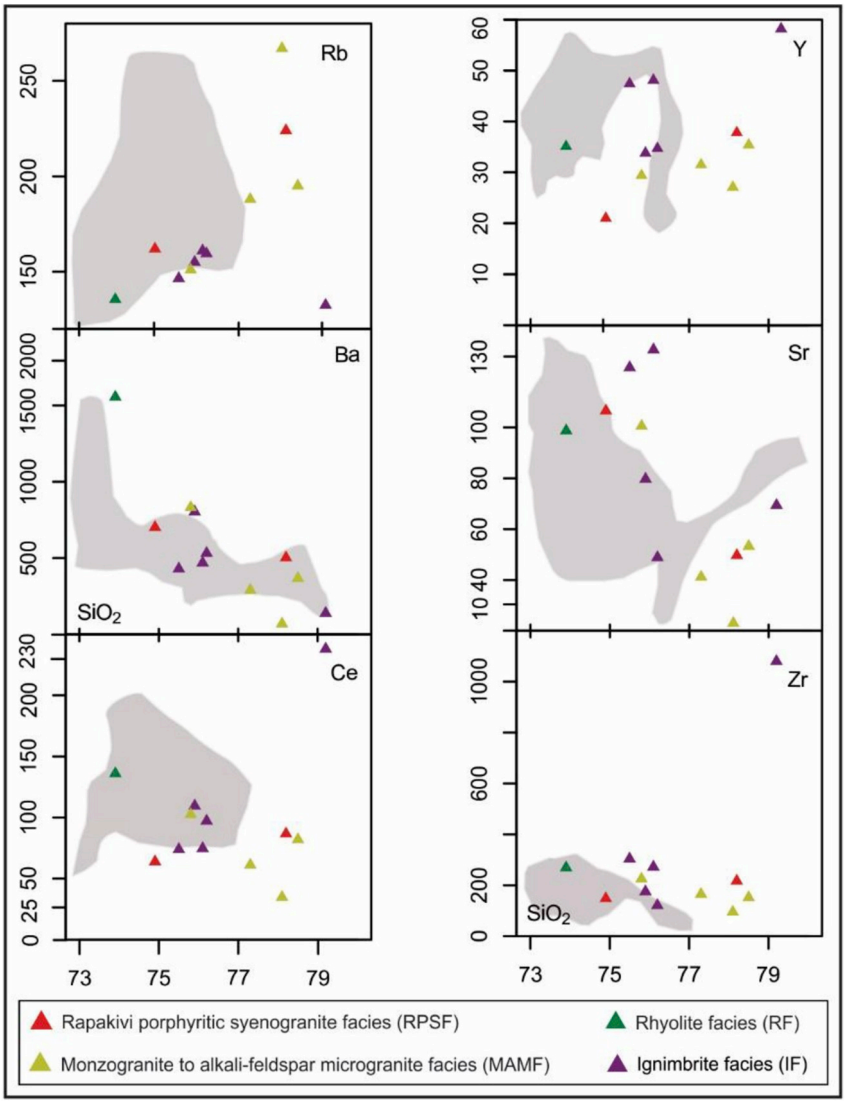

Fig. 11. Harker (1909) diagram with the distribution of data of trace elements (in ppm) of the CS rocks. Gray fields: CS geochemical data published by Cubas et al. (1998).

values. The decrease of light REE content observed in two samples may be due to the fractionation of allanite. According to Rollinson (1993), the allanite and monazite removal causes a decrease of these elements. The negative anomalies of Eu observed in all facies indicate the high grade of magma differentiation. The samples mostly show moderate negative Eu/Eu* anomalies with mean ratios of approximately 0.39, with wider ranges (from 0.05 to 0.60) in IF specimens (Fig. 12A), which have higher REE_{total} contents. MAMF samples show little heavy REE fractionation, negative Eu anomalies (Eu/Eu* ratio between 0.21 and 0.58) and one sample with a positive Ce anomaly (Fig. 12B), whereas the RPSF and RF samples showed moderate negative Eu anomalies (Eu/Eu* from 0.39 to 0.55; Fig. 12C and D).

The distribution diagrams of CS trace elements and K_2O, normalized using the granite values of the Ocean Ridge (Pearce et al. 1984) are shown according to the relative distribution of each facies (Fig. 13A–D). The samples show a selective enrichment of light-ion lithophile elements (LILEs) relative to the high-field strength elements (HFSEs), showing a model similar to those of volcanic arc granitoids. A sub-horizontal pattern is noted for Hf, Zr, Y and Yb, similar to that of high-K calc-alkaline granitoids of the Andean magmatic arc. Negative Nb and Ta anomalies in all facies suggest crustal contamination (Rollinson, 1993). Kelemen et al. (1993) indicate that Nb negative anomalies are related to upper mantle melting in settings related to magmatic arc development. Ce shows little fractionation in relation to adjacent elements, suggesting a possible proximity to hydrothermal sources (Munhá and Kerrich, 1980). Except for the RF, Ba negative anomalies found in the other facies suggest feldspar fractionation. This lack of Ba anomaly can be explained by the scarcity of plagioclase, apatite and/or biotite in RF.

Discriminating diagrams, proposed by Whalen et al. (1987), which use the 10.000*Ga/Al *versus* Zr and FeO_t/MgO ratios and Zr + Nb + Ce + Y *versus* FeO_t/MgO diagrams, are shown in Fig. 14. The values of the 1000*Ga/Al ratio are always higher than 2.6, and the Zr + Nb + Ce + Y, higher than 350, characterize the study rocks as A-type granitoids.

In the Nb−Y−Ce diagram proposed by Eby (1992; Fig. 15A), the points representing CS samples coincide with the A2 domain of A-type granites, with high values of the Y/Nb ratio, which suggests magmatism from a crustal source. Eby (1992, 2006) suggests an origin related to the differentiation of tholeiitic basalts with varying degrees of crustal interaction, by partial melting of crustal sources previously submitted to a melting episode. The A2 group includes granitoids found in several tectonic environments, such as the typical rapakivi granites, which are A-type granitoids derived from alkaline magmas positioned in post-

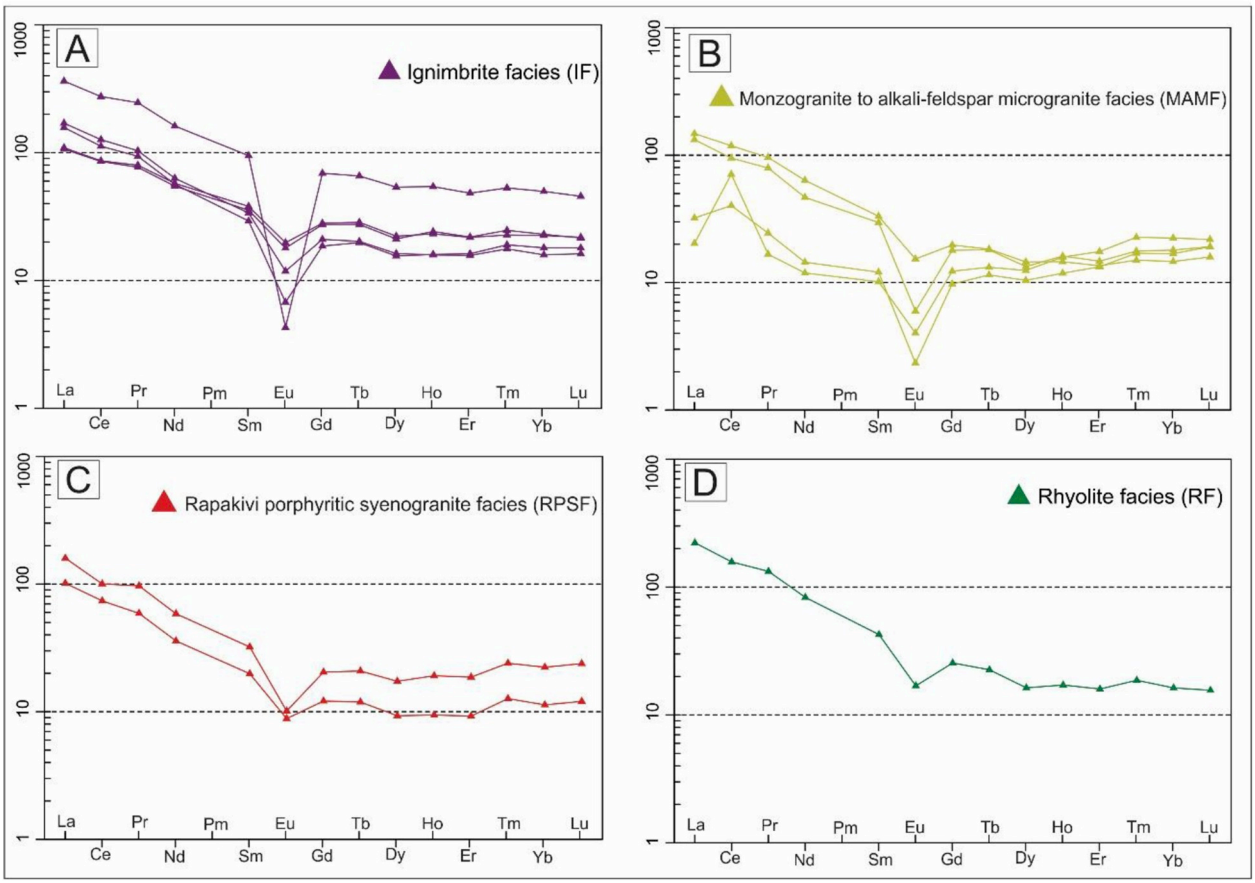

Fig. 12. Patterns data of CS rare earth elements, normalized using the chondritic values of Nakamura (1974).

tectonic, or even anorogenic, environments, according to the definition by Loiselle and Wones (1979). In the discriminating plots of tectonic environments proposed by Harris et al. (1986; Fig. 15B) and by Pearce et al. (1984) and then modified by Pearce (1996; Fig. 15C), the samples are plotted in the fields delimited for Phanerozoic granitoids of volcanic and post-collisional arc environments, respectively.

4.3. Geochronology U–Pb (in zircon)

Extrusive and intrusive members of two of the four facies identified that best represent the Caapucú Suite were selected for geochronological analysis using the U–Pb-zircon method. The rapakivi porphyritic syenogranite facies (AG04) and ignimbrite facies (AG06) are located in the southern and northern regions of the study area, respectively (Fig. 3).

Sample AG04 is pink and fine-to-medium grained with a syenogranitic composition and porphyritic texture. The zircon crystals of this sample are colorless to brownish yellow, with sizes usually ranging from 150 to 250 μm, although crystals smaller than 100 μm and larger crystals, ranging from 300 to 400 μm, also occur. The most abundant are euhedral and show prismatic habits, with well-defined pyramids.

Sample AG06 is reddish-brown and has a felsitic composition, with fine-to-very-fine grained and rich in feldspar and quartz crystals. The zircon grains range from colorless to dark-to-light yellow and, sometimes, tinted, commonly euhedral with the prismatic habit. The most abundant percentage shows sizes ranging from 50 to 180 μm, and they rarely occur in sizes ranging from 200 to 300 μm. Crystals smaller than 50 μm are also observed.

Images were acquired using scanning electron microscopy (SEM), cathodoluminescence (CL) and back-scattered electron microscopy (BSE). The 11 crystals analyzed in these images are long prisms with well-developed terminations, which is commonly found in the grains of most magmatic rocks (Vavra et al. 1996). Their sizes range from 80 to 300 μm, and they show relatively regular light and dark zoning bands representing different contents of uranium. They show 2/1 and 3/1 length *versus* width ratio (Fig. 16), with an elongated morphology in the x-axis relative to the y-axis, following the morphology indicated by Pupin (1980) for zircons of igneous rocks. The crystal in Fig. 16F is an exception.

The crystals generally exhibit low contrast between individual growth zones and growth sectors, interpreted as the portions of continuous magmatic development of the zircon crystals (Vavra et al. 1996). However, grains A, C and D show a significant contrast in their expansions due to a large, uniform, central zone succeeded by thin zoned bands at the edges. Low-to-medium luminescence rates are observed in the cores of crystals C, G and H.

According to Vavra (1994), zircon crystals grow as pyramids due to crystallization during a period with a constant and high cooling rate. These authors suggest that the morphology in very steep pyramids of the crystals is characteristic of granitoids derived from alkaline magmatism.

Corfu et al. (2003) explain that the zoning of the zircon crystals results from crystal growth interruption and reabsorption of the original zoning, succeeded by new depositions. This phenomenon develops due to the kinematics of large-scale magma mixing, which causes periods of Zr sub-saturation in the liquid.

According to Xiang et al. (2011), the U and Th levels of the zircon of magmatic origin change with the increase in temperature, increasing the Th content relative to the U content in the magma. Therefore, the high Th/U ratios are likely related to the degree of liquid disequilibrium during zircon crystallization. The geochronological data are presented in Table 6.

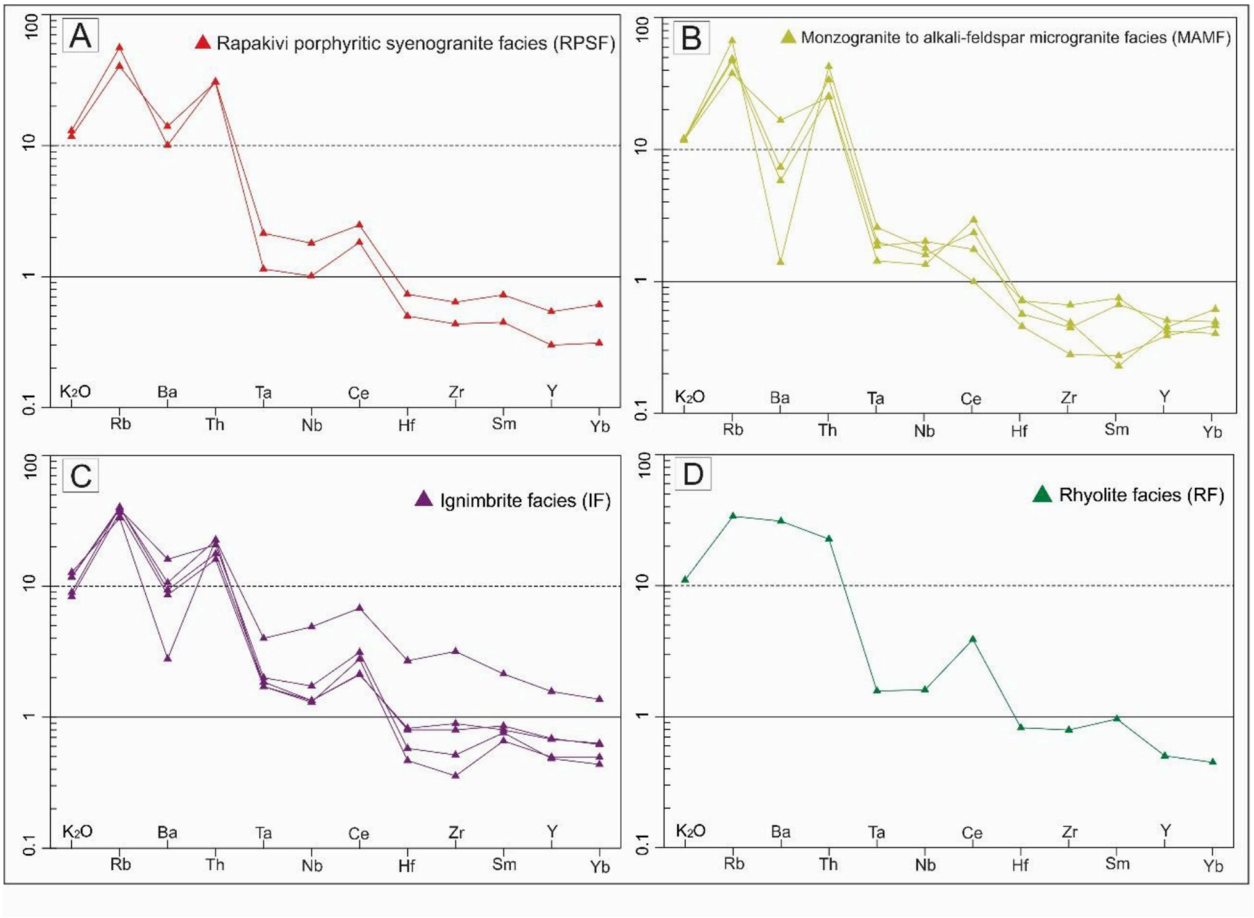

Fig. 13. Distribution of data of CS trace elements and K_2O, normalized using the granite values of the Ocean Ridge Granites (Pearce et al. 1984).

In sample AG04, 32 crystals were analyzed, of which 21 resulted in an upper intercept age of 563.7 ± 7.9 Ma with a 1.13 Mean Square of Weighted Deviates (MSWD; Fig. 17A), considered as the age of crystallization of the rock. Of these, 6 crystals yielded a concordant age of 543 ± 7.3 Ma, with 1.4 MSWD (Fig. 17B).

In sample AG06, 25 crystals were analyzed, of which 23 generated an upper intercept age of 565 ± 11 Ma, with 1.15 MSWD (Fig. 17C), interpreted as the age of crystallization. Of these crystals, 5 yielded a concordant age of 553.1 ± 5.4 Ma, with 1.5 MSWD (Fig. 17D).

5. Discussions

CS is composed of an association of acid plutonic and volcanic (effusive and explosive) rocks of monzogranitic to syenogranitic composition and very-fine-to-medium grained with a porphyritic and inequigranular texture. The occurrence of perthitic alkali feldspars and sodic plagioclase (albite to oligoclase) as isolated phase characterizes the study rocks as subsolvus granites.

Ignimbrites are pyroclastic deposits originated under high temperature conditions and from flow of pumices, independent of grain size, degree of welding or volume of the deposit (Sparks et al. 1973). The presence of crystalloclasts in IF indicates an origin from liquids with high crystallization rate, and the intense fragmentation identified suggests impact along the magmatic conduit or turbulent surface transport (McPhie et al. 1993). In general, lithic fragments derived from pre-existing rocks are absent or sparse in lava flows and syn-volcanic intrusions (McPhie et al. 1993).

Glass subjected to prolonged heat, pressure and solutions would be granophyric, consisting of fine, equigranular quartz and feldspar, which are products of devitrification (Lofgren, 1971b), as the micropoikilitic

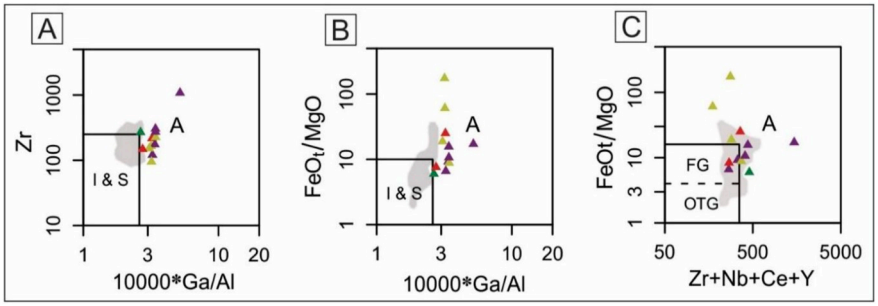

Fig. 14. Distribution of data of representing CS in the Whalen et al. (1987) diagrams for granitoid classification. Gray fields: CS geochemical data published by Cubas et al. (1998).

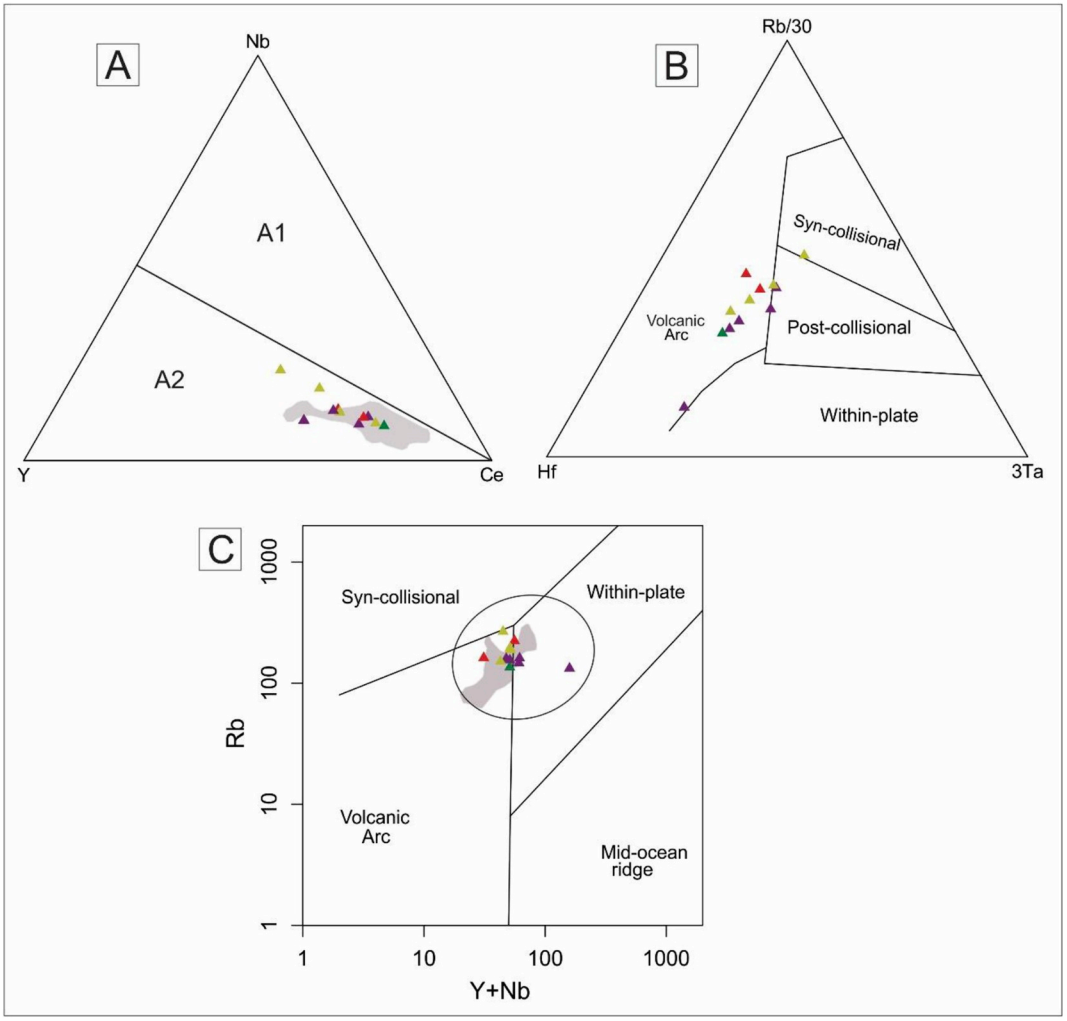

Fig. 15. Distribution of data of representing the CS rocks in the following diagrams: (A) Y—Nb—Ce (Eby, 1992); (B) Hf—Rb/30-3Ta (Harris et al.1986) and (C) Y + Nb *versus* Rb proposed by Pearce et al. (1984) and Pearce (1996). Gray fields: CS geochemical data published by Cubas et al. (1998).

texture. This texture occurs mainly in rocks of silicic composition (McPhie et al. 1993) and may result from initial cooling of glass (Anderson, 1969). According to McPhie et al. (1993), rates of devitrification are very slow below 300 °C under dry conditions, or presence of pure water.

The bight and corrosion gulfs commonly identified in phenocrysts of plutonic facies must have occurred during magma ascent and overflow. According to McPhie et al. (1993), SiO_2 solubility increases with decreasing pressure, as phenocrysts that are initially in equilibrium with the liquid are now partially reabsorbed.

The constant presence of the granophyric texture may indicate shallow level of emplacement for the intrusive rocks in this suite because the texture is generated by fast and simultaneous crystallization of quartz and alkali feldspar in a magmatic liquid (Smith, 1974). Whalen et al. (1987) indicated that a granophyric texture is common among epizonal granitic bodies, particularly among those associated with volcanic rocks. This texture is commonly found in alkaline granites, such those occurring in intracontinental rift environments (Whalen et al. 1987).

According to Bonin (1998), the genesis of granitic complexes at low depths is usually associated with A-type granitic liquid rises, which are favored by the density contrast between the magma and the host rocks as well as by differentiation processes. Gill (2014) suggested that ring-shaped intrusions may indicate subsidence of much larger crustal blocks, which are a key channel for the rise of acidic magma in the upper crust.

Geochemically, the rocks are represented by acid terms, the volcanic facies ranging from rhyolite to alkali rhyolite and the plutonic facies from granite to alkali granite. Whalen et al. (1996) suggested that volcano-plutonic associations with a geochemical affinity that is compatible with A-type magmas are commonly found. Vavra (1994) affirm that Nb, Zr and Y depletion may indicate the alkaline origin of the rock. Sr and Ba are negatively correlated with the SiO_2 index, suggesting feldspar fractionation and a high rate of magma differentiation (Vavra, 1994), as the negative anomalies of Eu.

Rapakivi granites commonly occurs forming ring complexes and coexist with biotite, peraluminous granites and alkaline granites (Wernick, 2004). According to Ramo and Haapala (1995), the term rapakivi granites is used for anorogenic or post-tectonic A-type granites with rapakivi textures. Also according to these authors, the origin of rapakivi granites may be related to melting by dehydration of the biotite and/or amphibole of crustal protoliths and to fractionation of mantle magmas. Bonin (2007) affirm that A-type complexes are mostly emplaced within stable and cooling areas of thickening lithosphere. Therefore, the CS was likely derived from a large-scale mantle rise, allowing for partial melting of the crust.

U—Pb geochronological data reveal a crystallization age of the CS-forming magma of 563 ± 7.9 Ma and 565 ± 11 Ma for the RPSF

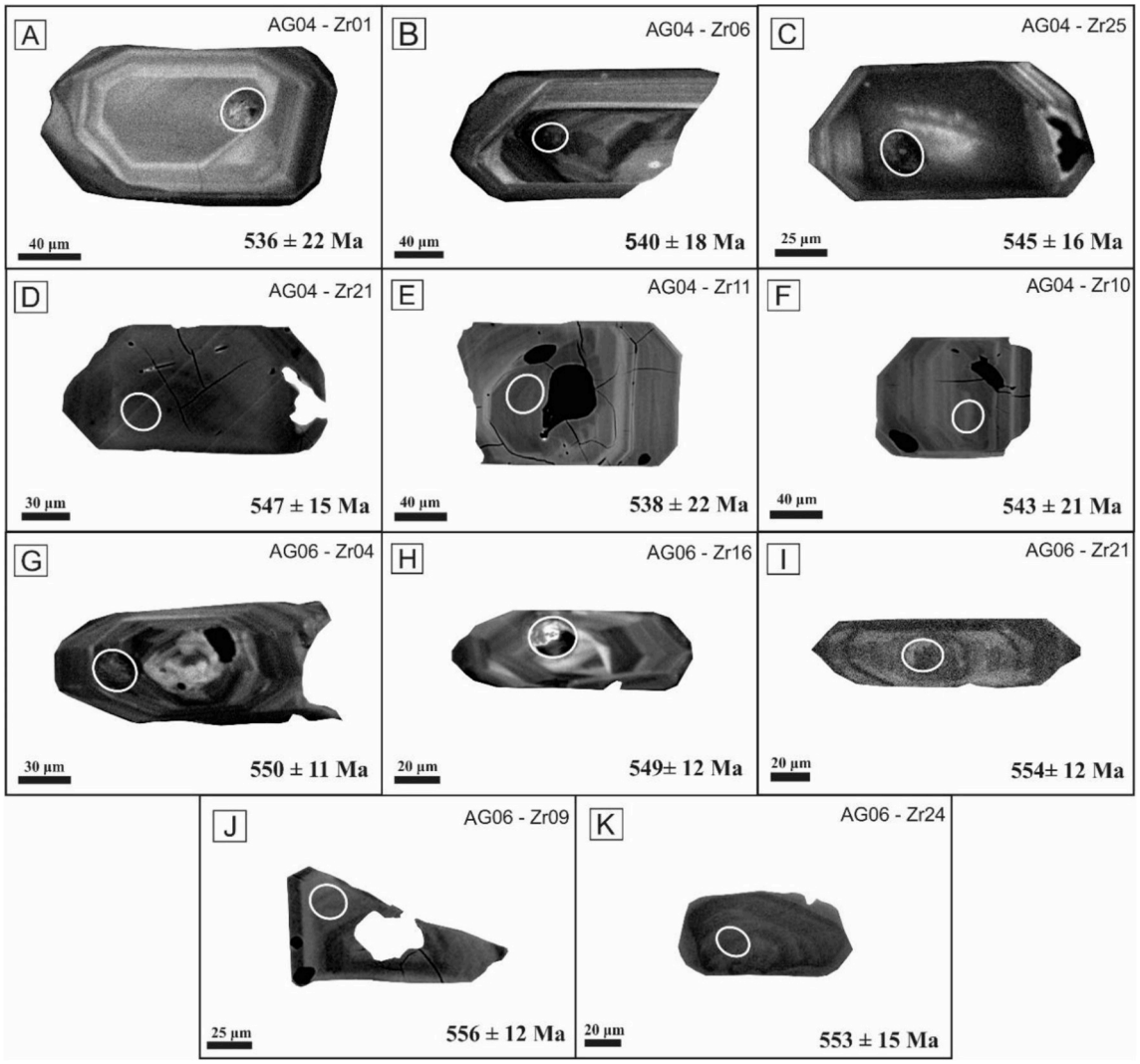

Fig. 16. Representative images of zircon crystals of samples AG04 (A to F) and AG06 (G to K). Crystals A, B, C, G, H and I are shown in CL images and crystals D, E, F, J and K are shown in BSE images. The white circles indicate the positions of spots, approximately 30 µm in diameter, produced by laser ablation.

(AG04) and IF (AG06) samples, respectively. Therefore, these ages correlate with the period that followed The Braziliano orogenesis. The association of the rocks is confirmed by the similarity of their geochemical behavior and U—Pb ages, indicating that both originated during the same volcano-plutonic event. It should be noted that the ages obtained in this study corroborate with the Rb—Sr results reported by Cordani et al. (2001), with an initial $^{87}Sr/^{86}Sr$ ratio of 560 ± 35 Ma.

Meira et al. (2015) indicated that the mobile belts of the Mantiqueira Province in Brazil originated from an intracontinental orogeny driven by the propagation of the collision between the Paranapanema and São Francisco cratons at approximately 650–600 Ma, followed by extensional tectonism and voluminous post-orogenic granitic magmatism at 600-560 Ma. Thus, the findings above suggest that the CS magmatism developed in the final stage of formation of the Paraguari mobile belt, generated by the cratonic collision between Paranapanema and Rio de La Plata cratons (Ruiz et al. 2018). Therefore, it is possible that the mobile belts of the Mantiqueira Province and the Paraguari mobile belt were generated during the same orogenetic event (Fig. 18).

Therefore, the middle Ediacaran to early Cambrian throughout West Gondwana is characterized by widespread extension recorded by rift-related basins, epicontinental sea deposits and voluminous post-orogenic magmatism (Pimentel et al., 1996; Janasi et al., 2009; Meira et al. 2014, 2015). Almeida et al. (2010, 2012) proposed a tectonic model, which was described as a more than 1500 km-long continuous regional system along the southern and central part of the Mantiqueira Province.

A-type granitoids in post-collisional environments are associated with large regional faults (Sylvester, 1989). According to gravimetric studies conducted by Dragone et al. (2017), geological evidence marking suture zones of the Paranapanema Craton includes the presence of Neoproterozoic granites bordering the mobile belts, for example, in the Caapucú Suite (Cubas et al. 1998), and granites of the Dom Feliciano Suite (Philipp and Machado, 2005).

6. Conclusions

CS represent an acid and isotropic igneous exposition in the Alto Caapucú Block. The detailed petrographic study of the samples allowed the CS classification in facies. Four facies were distinguished based on differences in color, particle size, mineralogical composition and textures. All the facies present leucocratic character. The plutonic facies (RPSF and MAMF) show monzogranitic to syenogranitic composition

Table 6
Results of the U–Pb (LA-ICPMS) analysis of zircon of samples AG04 and AG06.

Sample	Cristal	ƒ 206%	Th/U	$^{206}Pb/^{204}Pb$	$^{207}Pb/^{206}Pb$	1 ó (%)	$^{207}Pb/^{235}U$	1 ó (%)	$^{206}Pb/^{238}U$	1 ó (%)	Apparent Ages (Ma)						Rho	% U–Pb (Disc)
											$^{207}Pb/^{206}Pb$	2 ó	$^{207}Pb/^{235}U$	2 ó	$^{206}Pb/^{238}U$	2 ó		
AG04 (concordant)	037-ZR25	0,0009	0,496	30232	0,05876	1,39	0,715	2,10	0,0882	1,53	558	60	548	18	545	16	0,73	2.38
	033-ZR21	0,0011	0,658	144769	0,05919	1,24	0,722	1,94	0,0885	1,44	574	54	552	16	547	15	0,74	4.79
	018-ZR11	0,0009	0,540	43109	0,05879	1,87	0,706	2,86	0,0871	2,13	559	81	542	24	538	22	0,74	3.81
	017-ZR10	0,0009	0,410	35167	0,05838	1,87	0,707	2,77	0,0878	2,01	544	81	543	23	543	21	0,73	0.27
	010-ZR06	0,0009	0,553	33112	0,05943	1,74	0,716	2,5	0,0873	1,76	583	75	548	21	540	18	0,70	7.39
	004-ZR01	0,0005	0,717	27526	0,05792	1,82	0,692	2,83	0,0866	2,13	527	79	534	23	536	22	0,75	−1.66
AG04 (discordant)	035-ZR23	0.0150	0.614	479419	0.05857	0.65	0.776	1.19	0.0961	0.93	551	28	583	11	592	11	0.78	−7.31
	034-ZR22	0.0132	0.462	349413	0.05853	0.73	0.768	1.36	0.0952	1.09	550	32	579	12	586	12	0.80	−6.68
	029-ZR19	0.0087	0.539	401754	0.05828	0.83	0.774	1.35	0.0963	1.00	540	36	582	12	593	11	0.74	−9.69
	026-ZR16	0.0155	0.727	640923	0.05811	0.51	0.776	1.09	0.0968	0.89	534	22	583	10	596	10	0.82	−11.58
	025-ZR15	0.0122	0.458	8506	0.05948	0.76	0.796	1.23	0.0971	0.89	585	33	595	11	597	10	0.73	−2.14
	013-ZR07	0.0125	0.319	18818	0.05889	0.82	0.773	1.39	0.0952	1.06	563	35	582	12	586	12	0.76	−4.15
	014-ZR08	0.0294	1.020	1134822	0.05782	0.69	0.763	1.24	0.0956	0.96	523	30	576	11	589	11	0.78	−12.57
	028-ZR18	0.0118	0.455	6975	0.06022	0.80	0.791	1.33	0.0953	1.00	612	34	592	12	587	11	0.75	4.08
	006-ZR02	0.0010	0.586	44243	0.05861	1.30	0.754	2.04	0.0932	1.53	553	56	570	18	575	17	0.75	−3.97
	042-ZR30	0.0006	0.530	26240	0.05836	2.69	0.744	3.68	0.0924	2.47	543	116	565	32	570	27	0.67	−4.93
	007-ZR3	0.0017	0.430	52126	0.05923	1.03	0.735	1.63	0.0900	1.21	576	44	560	14	556	13	0.74	3.49
	005-ZR02	0.0005	0.639	22932	0.05893	2.60	0.676	3.85	0.0832	2.81	565	111	525	31	515	28	0.73	8.73
	038-ZR26	0.0017	0.556	75354	0.05877	0.98	0.723	1.54	0.0892	1.13	559	42	552	13	551	12	0.73	1.42
	020-ZR13	0.0019	0.566	35916	0.05974	0.95	0.709	1.43	0.0860	1.00	594	41	544	12	532	10	0.70	10.47
	030-ZR20	0.0013	0.537	60131	0.06003	1.64	0.723	2.29	0.0874	0.93	605	70	553	19	540	16	0,68	10,67
AG06 (concordant)	006-ZR04	0,0007	0,644	18510	0,05933	0,81	0,729	1,38	0,0891	1,06	579	35	556	12	550	11	0,76	99,0
	013-ZR09	0,0009	0,429	70062	0,05854	0,89	0,727	1,50	0,0901	1,14	550	39	555	13	556	12	0,76	100,2
	020-ZR16	0,0006	1222	18010	0,05907	1,09	0,725	1,62	0,0890	1,14	570	47	553	14	549	12	0,70	99,3
	027-ZR21	0,0007	0,490	24446	0,05881	0,87	0,728	1,49	0,0897	1,15	560	38	555	13	554	12	0,77	99,8
	030-ZR24	0,0006	0,831	26323	0,05893	1,35	0,727	2,02	0,0895	1,46	564	58	555	17	553	15	0,72	99,6
AG06 (discordant)	038-ZR30	0.0003	0.558	13860	0.05848	1.13	0.733	1.84	0.0909	1.41	548	49	558	16	561	15	0.76	−2.42
	039-ZR31	0.0005	0.726	15101	0.05917	1.13	0.736	1.83	0.0903	1.39	573	49	560	16	557	15	0.76	2.81
	014-ZR10	0.0004	0.584	21173	0.05871	1.29	0.697	1.82	0.0861	1.23	556	56	537	15	533	13	0.68	4.26
	036-ZR28	0.0007	0.411	22617	0.05986	1.01	0.759	1.70	0.0919	1.32	599	44	573	15	567	14	0.77	5.29
	026-ZR20	0.0004	0.459	17581	0.05927	1.01	0.721	1.68	0.0882	1.28	577	44	551	14	545	13	0.77	5.56
	023-ZR17	0.0004	0.555	14281	0.05940	1.20	0.722	1.75	0.0881	1.22	582	52	552	15	544	13	0.70	6.42
	005-ZR03	0.0005	0.542	69283	0.05957	1.74	0.719	2.12	0.0875	1.15	588	75	550	18	541	12	0.54	8.01
	037-ZR29	0.0002	0.726	8622	0.05943	1.46	0.707	2.04	0.0863	1.37	583	63	543	17	534	14	0.67	8.44
	004-ZR02	0.0004	0.830	14557	0.05986	1.14	0.724	1.74	0.0877	1.26	598	49	553	15	542	13	0.73	9.48
	018-ZR14	0.0005	0.669	11819	0.05997	1.23	0.720	1.68	0.0871	1.09	602	53	551	14	538	11	0.65	10.67
	010-ZR08	0.0004	0.408	15237	0.06030	1.30	0.735	1.75	0.0884	1.11	614	56	560	15	546	12	0.64	11.11
	028-ZR22	0.0003	0.471	12764	0.06004	1.66	0.714	2.30	0.0863	1.54	605	71	547	19	534	16	0.67	11.82
	040-ZR32	0.0003	0.456	12994	0.06073	1.75	0.752	2.30	0.0898	1.45	630	75	569	20	554	15	0.63	11.98
	007-ZR05	0.0005	0.476	11335	0.06094	1.15	0.758	1.59	0.0902	1.03	637	49	573	14	557	11	0.65	12.64
	035-ZR27	0.0002	0.406	5158	0.06042	1.88	0.719	2.61	0.0863	1.78	619	80	550	22	534	18	0.68	13.74
	008-ZR06	0.0003	0.606	13468	0.06088	1.14	0.739	1.69	0.0880	1.18	635	49	562	15	544	12	0.70	14.38
	033-ZR25	0.0003	0.584	8844	0.06057	1.36	0.718	2.28	0.0860	1.78	624	58	550	19	532	18	0.78	14.78
	025-ZR19	0.0003	0.804	10496	0.06156	1.45	0.759	2.14	0.0894	1.52	659	62	573	19	552	16	0.71	16.22

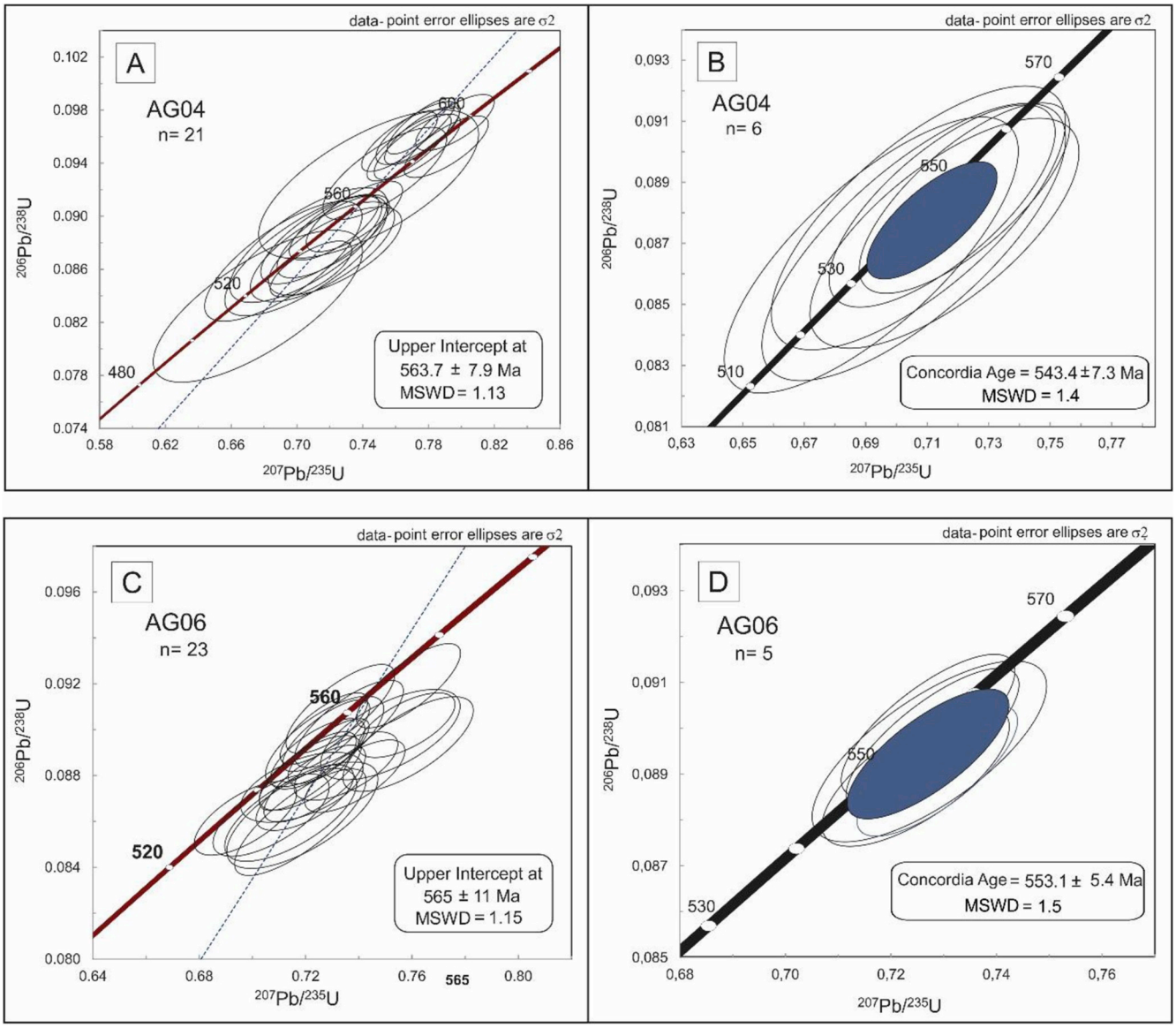

Fig. 17. (A) U–Pb diagram with the upper intercept age for sample AG04; (B) U–Pb concordia age diagram of sample AG04; (C) U–Pb diagram with the upper intercept age for sample AG06; and (D) U–Pb concordia age diagram of sample AG06.

with the occurrence of porphyritic, perthitic and granophyric textures. The volcanic facies are subdivided in effusive (RF) and explosive (IF) and show a quartzo-feldspatic aphanitic matrix and porphyritic texture. RF presents a porphyritic texture and lithoclasts (less than 5%), which are cognate of the rhyolitic rocks. IF displays fractured crystalloclasts and lithic fragments. Occasionally the matrix shows the micropoikilitic texture, as product of devitrification. Fiammes are common in the planar foliation, displaying eutaxitic texture.

CS represents a volcanic-plutonic magmatic association in which compositional variation originated at different stages of emplacement and crystallization in the crust. Based on lithochemical data, the magmatism responsible for the formation of CS yields a ferrous signature and metaluminous to slightly peraluminous character, generating A-type granitoids in a post-collisional arc environment. The REE patterns of the facies are similar to those observed in A-type magmatism related with post-collisional settings. The Nb and Ta negative anomalies in trace elements, as well as the LREE enrichment in spidergrams, indicate a subduction modified mantle source. Moreover, the Ba anomaly suggest feldspar fractionation and the enrichment in Rb and Ce of these rocks suggest crustal participation in the sources.

The geochemical trends associated with 563 ± 7.9 Ma and 565 ± 11 Ma ages suggest that the genesis of CS be directly related to Meira et al.'s (2015) model, which in a 600-560 Ma period the study area underwent decompression associated with orogenic collapse. A tectonic-magmatic correlation of CS with post-tectonic igneous episodes of the Ribeira and/or Dom Feliciano belts of the Mantiqueira Province is also suggested.

Based on the above discussion, the CS was likely formed by post-collisional magmatism resulting from convergence and collision between the Paranapanema and Rio de la Plata cratons, related to the final stage of the evolution of Paraguari Belt, at Brazilian/Pan-African Cycle in the South American Platform, during the assembly of Western Gondwana.

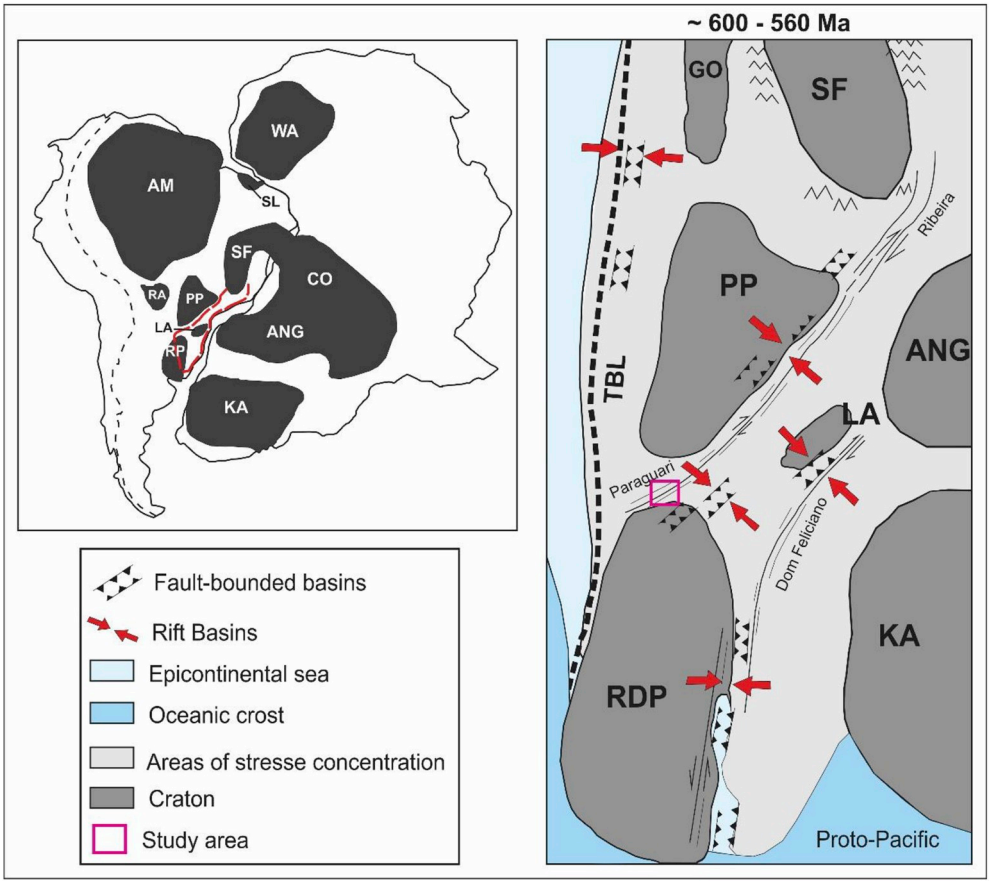

Fig. 18. Representative scheme indicating the preferred amalgamation trends among the eastern Gondwana cratons and the location of the Paraguari mobile belt. GO - Goiás Block; ANG – Angola Block; CO - Congo Craton; KA – Kalahari Craton; LA - Luis Alves Craton; PP: Paranapanema Craton; RA – Rio Apa Block; RP: Rio de La Plata Craton; SF: São Francisco Craton; SL – São Luis Craton; WA –West África Craton; TBL – Trans Brazilian Lineament (modified from Meira et al. 2015).

Acknowledgements

The authors wish to thank to the technicians of the Laboratory of Geochronology of the University of Brasília; to the editor (C. Montes) and reviewers for contributions and suggestions, and to Fundação de Amparo a Pesquisa do Estado de Mato Grosso (FAPEMAT) and Coordenação de Aperfeiçoamento de Pessoal de Nível Superior (CAPES) for financial support.

Appendix A. Supplementary data

Supplementary data to this article can be found online at https://doi.org/10.1016/j.jsames.2018.09.016.

References

Almeida, R.P., Janikian, L., Fragoso- Cesar, A.R.S., Fambrini, G.L., 2010. The Ediacaran to Cambrian rift system of Southeastern South America: tectonic implications. J. Geol. 118, 145–161.
Almeida, R.P., Santos, M.G.M., Fragoso-Cesar, A.R.S., Janikian, L., Fambrini, G.L., 2012. Recurring extensional and strike-slip tectonics after the Neoproterozoic collisional events in the southern Mantiqueira province. An. Acad. Bras. Cienc. 84, 347–376.
Almeida, F.F.M., Hasui, Y., 1984. O Precambriano Do Brasil. pp. 378 (São Paulo).
Anderson Jr., J.E., 1969. Development of a snowflake texture in a welded tuff, Davis Mountains, Texas. Geol. Soc. Am. Bull. 80, 2075–2080.
Barreto, G.S., 2016. Geologia dos granitos porfiríticos de Ilhabela – Petrogênese e evolução crustal. Dissertação de mestrado em geotectônica – Instituto de Geociências, Universidade de São Paulo, São Paulo Avaliabe at: http://tese.usp.br.
Bitschene, P.R., Lippolt, H.J., 1986. Acid magmatites of the Brasiliano cycle in east Paraguay. Zbl. Geol. Palaont., Teil I 9/10, 1457–1468.
Bittencourt, M.F., Nardi, L.V.S., 2000. Tectonic settings and sources of magmatismrelated to the southern shear belt. Rev. Bras. Geociencias 30 (1), 186–189.
Bonin, B., 1998. Alkaline rocks and geodynamics: transactions. J. Earth Sci. 7, 105–118.
Bonin, B., 2007. A-type granites and related rocks; evolution of a concept, problems and prospects. Lithos 97, 1–29.
Bühn, B., Pimentel, M.M., Matteini, M., Dantas, E.L., 2009. High spatial resolution analysis of Pb and U isotopes for geochronology by laser ablation multi-collector inductively coupled plasma mass spectrometry (LA-MC-ICP-MS). An Acad. Bras Ciências 81, 1–16.
Comte, D., Hasui, Y., 1971. Geochronology of eastern Paraguay by the potassium-argon method. Rev. Bras. Geociencias 1, 33–43.
Chaney, R., Stanley, D., Franco, R., 1982. Paso Pindó area. The anschutz Co. TAC Int. Rep.. Archivo DRM-MOPC, Assunción.
Cordani, U.G., Brito Neves, B.B., Fuck, R.A., Porto, R., Thomaz Filho, A., da Cunha, F.M.B., 1984. Estudo preliminar de integração do Pré-Cambriano com os eventos tectônicos das bacias sedimentares brasileiras, Petrobras, Cenpes, Sintep III. Série Ciência-Técnica-Petróleo 15, 1–70.
Cordani, U.G., Cubas, N., Sato, K., Nutman, A.P., Gonzales, M., Presser, J.L.B., 2001. Geochronological constraints for the evolution of the metamorphic complex near the Tebicuary River. In: Southern Precambrian Region of Paraguay. III Simposio Sudamericano de Geologia Isotopica, Pucon - Chile.
Cubas, N., Garcete, A., Meinhold, K.D., Benitez, J.C., Figueredo, L., Gonzales, M.E., Burgaht, K.P., Höhndorf, A., 1998. Mapa Geológico de la República del Paraguay. Escala 1:100 000, Hoja Villa Florida. MOCP, Asunción, pp. 71.
Corfu, F., Hanchar, J.M., Hoskin, P.W.O., Kinny, P., 2003. Atlas of zircon textures. Rev. Mineral. Geochem. 53, 469–500.
Dragone, G.N., Naomi, U., Gimenez, M.E., Klinger, F.G.L., Chaves, C.A.M., 2017. Western Paraná suture/shear zone and limits of Rio Apa, Rio Tebicuary and Rio de la Plata cratons from gravity data. Precambrian Res. 291, 162–177.
Eby, G.N., 1992. Chemical subdivision of the A- type granitoids: petrogenetic and tectonic implication. Geology 20, 641–644.
Eby, G.N., 2006. Distinction between A-type granites and petrogenetic pathways. In: Belém, Brazil. CD-ROM.
Eckel, E.B., 1959. Geology and mineral resources of Paraguay, A reconnaissance. Geol. Survey Prof. Paper. Washington 327, 110.
Favetto, A., Rocha, V., Pomposiello, C., Garcia, R., Barcelona, H., 2015. A new limit for the NW Río de la Plata Craton Border at about 24°S (Argentina) detected by Magnetotellurics. Geologica Ata 13 (3), 243–254.
Fulfaro, V.J., Palmieri, J.H., 1986. Proyeto Paraguay 83/005. Mapa Geológico del Paraguay (1:1.00.000 y texto explicativo). Governo República del Paraguay/ONU, Assunción, Paraguay.
Fulfaro, V.J., 1996. Geologia del Paraguay Oriental. Edusp/Fapesp, Sao Paulo, pp. 17–29.
Fragoso Cesar, A.R.S., 1991. Tectônica de placas no Ciclo Brasiliano: As orogenias dos Cinturões Dom Feliciano e Ribeira no Rio Grande do Sul. Tese de Doutorado – Instituto de Geociências, Universidade de São Paulo, São Paulo 362pp.
Frost, C.D., Frost, B.R., 1997. High-K, iron-enriched rapakivi-type granites: the tholeiite connections. Geology 25, 647–650.

Frost, B.R., Arculus, R.J., Barnes, C.G., Collins, W.J., Ellis, D.J., Frost, C.D., 2001. A geochemical classification of granitc rocks. J. Petrol. 42, 2033–2048.
Gasparini, P., Mantovani, M.S.M., 1979. Geochemistry of charnokites from São paulo state, Brazil. Earth Planet Sci. Lett. 42 (2), 311–320.
Gill, R., 2014. Rochas e processos ígneos: um guia prático. Porto Alegre, editora Bookman, pp. 252.
Harker, A., 1909. The Natural History of the Igneous Rocks. New York. pp. 384.
Harrington, H.J., 1950. Geologia do paraguai. Universidad de Buenos aires. Faculdad de Ciencias. Exactas y naturales. Contribuiciones científicas. Serie E. Geologia, Tomo 1, 82.
Harris, N.W.B., Pearce, J.A., Tindle, A.G., 1986. Geochemical characteristics of collision-zone magmatism. In: Coward, M.P., Ries, A.C. (Eds.), Collision Tectonics. vol. 19. Geological Society of London, Special Paper, pp. 115–158.
Janasi, V.A., Vlach, S.R.F., Campos Neto, M.C., Ulbrich, H.H.G.J., 2009. Associated A-type subalkaline and high-K calc-alkaline granites in the Itu Granite Province, southeastern Brazil: petrological and Tectonic significance. Can. Mineral. 47, 1505–1526.
Janousek, V., Farrow, C.M., Erban, V., 2006. Interpretation of whole-rock geochemical data in igneous geochemistry: introducing Geochemical Data Toolkit (GCDkit). J. Petrol. 47, 1,255–1,259.
Kanzler, A., 1987. The Southern Pre-Cambrian in Paraguay. Geological inventory and ages relations. Zbl. Geol. Palaont. Teil I 7/8, 753–765 Stuttgart.
Kelemen, P.B., Shimizu, N., Dunn, T., 1993. Relative depletion of niobium in some arc magmas and the continental crust: partitioning of K, Nb, La and Ce during melt/rock reaction in the upper mantle. Earth Planet Sci. Lett. 120, 111–134.
La Roche, H., Leterrier, J., Grandclaude, P., Marchal, M., 1980. A classification of volcanic and plutonic rocks using R1 R2 - diagrams and major element analyses-its relationships with current nomenclature. Chem. Geol. 29, 183–210.
Liaghat, S., MacLean, W.H., 1995. Lithogeochemistry of altered rocks at the new insco VMS deposit, noranda, quebec. J. Geochem. Explor. 52, 333–350.
Lofgren, G., 1971b. Experimentally produced devitrification textures in natural rhyolitic glass. Geol. Soc. Am. Bull. 82, 111–124.
Lohse, B., 1990. Petrographische und geochronologische Erkenntnisse über den Westteil des Tebicuary-Kratons. In: Südost Paraguay. Diplom. Diss., Univ. Heidelberg, 103 p.
Loiselle, M.C., Wones, D.R., 1979. Characteristics and origin of anorogenic granites. Geol. Soc. Am. Abs. Prog. 11 (3), 468.
Ludwig, K.R., 2003. Isoplot 3.00 - a Geochronological Toolkit for Microsoft Excel. Berkeley 1240 Geochronology Center, Special, Publication No 4.
Macluf, S., Schorscher, J.H.D., 2001. Petrogênese das rochas charnokiticas e aplitos intrusivos do Complexo Charnokitico e Ubatuba, SP. In: Simpósio de Geologia do Sudeste 7. Boletim de Resumos, Rio de Janeiro, pp. 46.
Maniar, P.D., Piccoli, P.M., 1989. Tectonic discrimination of granitoids. Geol. Soc. Am. Bull. 101, 635–643.
Mantovani, M.S.M., Brito Neves, B.B., 2005. The Paranapanema litospheric block: its importance for Proterozoic (Rodinia, Gondwana) supercontinent theories. Gondwana Res. 8, 303–315.
McPhie, J., Doyle, M., Allen, R., 1993. Volcanic Textures. A Guide to the Interpretation of Textures in Volcanic Rocks. Tasmanian Government Printing Office, Tasmania 198pp.
Meinhold, K.D., Cubas, N., Garcete, A., 2011. Mapa Geológico 1:250.000 del Complejo Precámbrico Sur del Paraguay, texto explicativo. pp. 22.
Meira, V.T., Juliani, C., Schorscher, J.H.D., Garcia-Casco, A., Hyppolito, T., 2014. Does the pico do papagaio batholith indeed represent a neoproterozoic magmatic arc? In: IX South American Symposium on Isotope Geology, Abstracts, São Paulo, Brazil.
Meira, V.T., Garcia-Casco, A., Juliani, C., Almeida, R.P., Schorscher, J.H.D., 2015. The role of intracontinental deformation in supercontinente assembly: insights from the Ribeira Belt, Southeastern Brazil (Neoproterozoic West Gondwana). Terra. Nova 27 (3), 206–217.
Milani, E.J., Ramos, V., 1998. Orogenias paleozoicas no domínio sul-ocidental do Gondwana e os ciclos de subsidência da Bacia do Paraná. Rev. Bras. Geociencias 28 (4), 473–484.
Munhá, J., Kerrich, R., 1980. Seawater – basalt interaction from the iberian pyrite belt. Contrib. Mineral. Petrol. 73, 191–200.
Nakamura, N., 1974. Determination of REE, Ba, Fe, Mg, Na and K in carbonaceous and ordinary chondrites. Geochem. Cosmochim. Acta 38, 757–775.
O'Connor, J.T., 1965. A classification for quartz-rich igneous rocks based on feldspar ratios. US Geol. Surv. 525B, 79–84.
Oliveira, D.S., 2015. Geologia e petrologia das rochas riolíticas do cerro Ana Dias. Dissertação de Mestrado – Instituto de Geociências, Universidade Federal do Rio Grande do Sul, região de Quitéria, sudeste do RS. Porto Alegre, pp. 59.
Pimentel, M.M., Fuck, R.A., Alvarenga, C.J.S., 1996. Post-Brasiliano (Pan African) high-K granitic magmatism in central Brazil: the role of late Precambrian/early Paleozoic extension. Precambrian Res. 80, 217–238.
Padilha, A.L., Vitorello, Í., Antunes, C.A., Pádua, M.B., 2015. Imaging threedimensional crustal condutivity structures reflecting continental flood basalt effects hidden beneath thick intracratonic sedimentary basin. J. Geophys. Res. Solid Earth 120, 4702–4719.
Paula, U.G.M., 2018. Grupo Paso Pindó: remanescente supracrustal da Faixa Paraguari – sul do Paraguai: implicações tectônicas. Exame de qualificação de mestrado. In: Programa de Pós-Graduação em Geociências, Faculdade de Geociências (FAGEO) - Universidade Federal de Mato Grosso.
Pearce, J.A., Harris, N.B.W., Tindle, A.G., 1984. Trace element discrimination diagrams for the tectonic interpretation of granitic rocks. J. Petrol. 25 (4), 956–983.
Pearce, J.A., 1996. Source and settings of granitic rocks. Episodes 19 (4), 120–125.
Philipp, R.P., Machado, R., 2005. The Late Neoproterozoic granitoid magmatism of the Pelotas Batholith, southern Brazil. J. S. Am. Earth Sci. 19, 461–478.
Philipp, R.P., Machado, R., Nardi, L.V.S., Lafon, J.M., 2002. O magmatismo granítico Neoproterozoico do Batólito Pelotas no sul do Brasil: novos dados e revisão da geocronologia regional. Rev. Bras. Geociencias 32 (2), 277–290.
Philipp, R.P., Pimentel, M.M., Chemale Jr., F., 2016. Tectonic evolution of the Dom Feliciano belt on southern Brazil: geological relationships and U-Pb geochronology. Braz. J. Genet. 46 (1), 83–104.
Presser, J.L.B., 1992. Geologia da Folha 5569- 111 La Colmena, Paraguai Oriental. Dissertação de Mestrado. IG-USP, São Paulo 205pp.
Pupin, J.P., 1980. Zircon and granite petrology. Contrib. Mineral. Petrol. 73, 207–220.
Putzer, H., 1962. Die Geologie von Paraguay – Beitrago Zur regionalen geologie der Erde, vol. 2. Ed. Gerbruder Borntraeger, pp. 183.
Ramo, O.T., Haapala, I., 1995. One hundred years of rapakivi granites. Mineral. Petrol. 52, 129–185.
Ramos, V., Dallmeyer, R.D., Vujovich, G., 1998. Time constraints on the early Palaeozoic docking of the Precordillera, central Argentina. In: In: Pankhurst, R.J., Rapela, C.W. (Eds.), The Proto-andean Margin of Gondwana, vol. 142. Geological Society of London, Special Publications, pp. 143–158.
Rapela, C.W., Pankhurst, R.J., Casquet, C., Fanning, C.M., Baldo, E.G., González-Casado, J.M., Galindo, C., Dahlquist, J., 2007. The Río de La Plata craton and the assembly of SW Gondwana. Earth Sci. Rev. 83, 49–82.
Rollinson, H., 1993. Using Geochemical Data: Evaluation, Presentation, Interpretation. Longman Scientific & Technical, UK Limited, Harlow, Essex, England, pp. 352p.
Ruiz, A.S., Cubas, N., Matos, J.B., 2018. Geological and geochronological evidences of Paraguari belt: a neoproterozoic orogen in Southern Paraguay. In: 11th South American Symposium on Isotope Geology.
Smith, J.V., 1974. Feldspar Minerals. Chemical and Textural Properties, vol. 2. Springer-Verlag, New York, pp. 690.
Sparks, R.S.J., Self, S., Walker, G.P.L., 1973. Products of ignimbrite eruptions. Geology 1, 115–118.
Sylvester, P.J., 1989. Post-collisional alkaline granites. J. Geol. 97 (3), 261–280.
Tupinambá, M., 1999. Evolução tectônica e magmática da Faixa Ribeira na região da Serra dos Órgãos. Tese de Doutoramento. Instituto de Geociências – Universidade de São Paulo, São Paulo, pp. 186 (unpublished).
Ulbrich, H.G.J., Vlach, S.R.F., Janasi, V.A., 2001. O mapeamento faciológico em rochas ígneas plutônicas. Rev. Bras. Geociencias 31 (2), 163–172.
Valeriano, C.M., Tupinambá, M., Simonetti, A., Heilbron, M., Almeida, J.C.H., Eirado, L.G., 2011. U–Pb LA-MC-ICPMS geochronology of Cambro-Ordovician postcollisional granites of the Ribeira Belt, southeast Brazil: terminal Brasiliano magmatism in central Gondwana supercontinent. J. S. Am. Earth Sci. 32, 415–428.
Vavra, G., 1994. Systematics of internal zircon morphology in major Variscan granitoid types. Contrib. Mineral. Petrol. 117, 331–344.
Vavra, G., Gebauer, D., Schim, R., Compostons, W., 1996. Multiple zircon growth and recrystallization during polyphase Late Carboniferous to Triassic metamorphism in granulites of the Ivrea Zone (Southern Alps): and ion microprobe (SHRIMP) study. Contrib. Mineral. Petrol. 122, 337–358.
Wernick, E., 2004. Rochas magmáticas: conceitos fundamentais e classificação modal, química, termodinâmica e tectônica – São Paulo, vol. 537 Editora UNESP.
Wiens, F., 1984. El precámbrico paraguayo. In: Simposio Nacional de Geologia. Resumen. Asunción.
Whalen, J.B., Currie, K.L., Chappel, B.W., 1987. A-type granites: geochemical characteristics, driscrimination and petrogenesis. Contrib. Mineral. Petrol. 95, 407–419.
Whalen, J.B., Jenner, G.A., Longstaffe, F.J., Robert, F., Gariépy, C., 1996. Geochemical and isotopic (O, Nd, Pb and Sr) constraints on A-type granite petrogenesis based on the topsails igneous suite, newfoundland appalachians. J. Petrol. 37 (6), 1463–1489.
Whitney, D.L., Evans, B.W., 2010. Abbreviations for names of rock-forming minerals. Am. Mineral. 95, 185–187.
Xiang, W., Griffin, W.L., Jie, C., Pinyun, H., Xiang, L., 2011. U and Th contents and Th/U ratios of zircon in felsic and mafic magmatic rocks: improved zircon-melt distribution coefficients. Acta Geol. Sin. 85 (1), 164–174.